Supporting Information

Insulated molecular wires: Inhibiting orthogonal contacts in metal complex based molecular junctions.

Oday A. Al-Owaedi,[a,bΘ] Sören Bock,[cΘ] David C. Milan,[dΘ] Marie-Christine Oerthel,[e] Michael S. Inkpen,[f] Dmitry S. Yufit,[e] Alexandre N. Sobolev,[c,g] Nicholas J. Long,[f] , Tim Albrecht,[f] Simon J. Higgins,[d] Martin R. Bryce,[e] Richard J. Nichols,[d]* Colin J. Lambert,[a]* Paul J. Low[c]*

[a] Department of Physics, University of Lancaster, Lancaster, LA1 4YB, UK

[b] Department of Laser Physics, Women Faculty of Science, Babylon University, Hilla, Iraq.

[c] School of Chemistry and Biochemistry, University of Western Australia, 35 Stirling Highway, Perth, 6009, Australia

[d] Department of Chemistry, University of Liverpool, Crown St, Liverpool, L69 7ZD, UK

[e] Department of Chemistry, Durham University, South Rd, Durham, DH1 3LE, UK

[f] Department of Chemistry, Imperial College London, London SW7 2AZ, UK

[g] Centre for Microscopy Characterization and Analysis, University of Western Australia, 35 Stirling Highway, Perth 6009, Australia

Email: r.j.nichols@liverpool.ac.uk, c.lambert@lancaster.ac.uk, paul.low@uwa.edu.au

EXPERIMENTAL SECTION

General conditions. All reactions were carried out in oven-dried glassware under oxygen-free argon atmosphere using standard Schlenk techniques. Diisopropylamine, diethylamine and triethylamine were purified by distillation from KOH, other reaction solvents were purified and dried using Innovative Technology SPS-400 and degassed before use. The compounds *cis*-$PtCl_2(PPh_3)_2$,[1] 2-trimethylsilylethynyl-5-ethynyl-1,4-bis(hexyloxy)benzene,[2] 1-ethynyl-4-trimethylsilylethynylbenzene,[3] and 1-trimethylsilylbuta-1,3-diyne[4] were prepared by literature methods. Other reagents and

intermediates were prepared by variations on literature methods as described below, or purchased commercially and used as received.

NMR spectra were recorded in deuterated solvent solutions on Varian 300 MHz, Bruker Avance 400 MHz, 500 MHz and 600 MHz or Varian VNMRS 700 MHz spectrometers and referenced against residual protio-solvent resonances ($CHCl_3$: ^1H 7.26 ppm, ^{13}C 77.16 ppm and CH_2Cl_2: ^1H 5.32 ppm, ^{13}C 53.84 ppm).[5] In the NMR assignment, the phenyl ring associated with the dppe and PPh_3 are denoted Ph and Ar indicates any arylene group belonging to the alkynyl ligands. The simpler spectra of the PEt_3 ligated complexes were fully assigned from 2D-NMR methods and detailed assignments are given for this series by way of example.

Matrix-assisted laser desorption ionization (MALDI) mass spectra were recorded using an Autoflex II TOF/TOF mass spectrometer with a 337 nm laser. Infrared spectra were recorded on a Thermo 6700 spectrometer from CH_2Cl_2 solution in a cell fitted with CaF_2 windows or an Agilent Technologies Cary 630 spectrometer using ATR sampling methods. High-resolution mass spectra were recorded using a Waters LCT Premier XE mass spectrometer using electrospray ionization with Leucine Enkephalin as reference.

Preparation of *cis-/trans*-$PtCl_2(PEt_3)_2$ [6]

A Schlenk flask was charged with 5 ml of degassed water followed by the addition of 5.9 g of 10 wt-% triethylphosphine solution in hexane (i.e. 0.59 g, 5 mmol PEt_3). To the stirred mixture, potassium tetrachloroplatinate (1.04 g, 2.5 mmol) was added. The mixture was stirred for 1.5 hours during which time an off-white coloured precipitate was formed. The hexane and other volatiles were removed under reduced pressure and the remaining aqueous suspension was heated to reflux for 2 hours. After cooling to room temperature, the precipitate was collected, washed with water and dried under vacuum. A

comparison of the spectroscopic data against literature data[7-9] indicated the product to be a mixture of *cis*- and *trans*-isomers of approximately 70:30 composition, which was used in the reactions described below without further purification. ^{1}H NMR ($CDCl_3$, 300MHz, δ / ppm): 1.06 - 1.24 (m, 25H, *cis* and *trans* C*H*$_3$), 1.80 - 1.93 (m, 5H, *trans* C*H*$_2$), 1.96 - 2.15 (m, 12H, *cis* C*H*$_2$). ^{31}P{^{1}H} NMR ($CDCl_3$, 122 MHz, δ / ppm): 10.2 (s, $J_{P\text{-}Pt}$ = 3516 Hz, *cis*), 13.3 (s, $J_{P\text{-}Pt}$ = 2384 Hz, *trans*).

Synthesis of *trans*-Pt{C≡CC$_6$H$_2$(Ohex)$_2$C≡CSiMe$_3$}$_2$(PPh$_3$)$_2$ (1a)

A solution of 2-trimethylsilylethynyl-5-ethynyl-1,4-bis(hexyloxy)benzene (48 mg, 0.12 mmol), *cis*-$PtCl_2(PPh_3)_2$ (50 mg, 0.06 mmol), copper iodide (1 mg, 0.01 mmol) in diethylamine (5 ml) was heated at reflux overnight. The resulting solution was dried and the residue was purified on silica column chromatography with gradient elution from CH_2Cl_2/hexane (1:1 v/v) to pure CH_2Cl_2. The main fraction was collected and the solvent removed to yield a yellow-colored, oily solid, which solidified upon precipitation by addition of a CH_2Cl_2 solution into MeOH (30 mg, 33%). ^{1}H NMR (CD_2Cl_2, 400 MHz, δ / ppm): 0.20 (s, 18H, Si*Me*$_3$), 0.86 - 0.93 (m, 12H, C*H*$_3$), 1.15 - 1.26 (m, 12H, C*H*$_2$), 1.33 - 1.37 (m, 12H, CH_2), 1.42 - 1.50 (m, 4H, C*H*$_2$), 1.65 - 1.72 (m, 4H, C*H*$_2$), 3.56 (t, *J* = 6.5 Hz, 4H, OC*H*$_2$), 3.63 (t, *J* = 6.5 Hz, 4H, OC*H*$_2$), 5.68 (s, 2H, Ar), 6.60 (s, 2H, Ar), 7.38 - 7.29 (m, 18H, Ph), 7.84 - 7.78 (m, 12H, Ph). ^{13}C{^{1}H} NMR ($CDCl_3$, 151 MHz, δ / ppm): 0.2 (s, $SiMe_3$), 14.3 (br s, *C*H$_3$), 22.7 (s, *C*H$_2$), 22.8 (s, *C*H$_2$), 25.6 (s, *C*H$_2$), 25.9 (s, *C*H$_2$), 29.2 (s, *C*H$_2$), 29.5 (s, *C*H$_2$), 31.7 (s, *C*H$_2$), 31.8 (s, *C*H$_2$), 69.2 (s, O-*C*H$_2$), 69.9 (s, O-*C*H$_2$), 97.8 (s, *C*≡ or *C*$_{Ar}$), 102.4 (s, *C*≡ or *C*$_{Ar}$), 108.8 (s, *C*≡ or *C*$_{Ar}$), 110.5 (s, *C*≡ or *C*$_{Ar}$), 117.2 (s, *C*$_{Ar}$-H), 118.2 (s, *C*$_{Ar}$-H), 121.2(s, *C*≡ or *C*$_{Ar}$), 127.7 (m, Ph$_m$), 130.2 (s, Ph$_p$), 131.4 (m, Ph$_i$),y 135.4 (m, Ph$_o$), 152.5 (s, O-*C*$_{Ar}$), 154.1 (s, O-*C*$_{Ar}$). A signal for Pt-*C* could not be observed. ^{31}P{^{1}H} NMR (CD_2Cl_2, 162 MHz, δ / ppm): 17.6 (s, $J_{P\text{-}Pt}$ = 2646 Hz). IR (CH_2Cl_2) ν_{max}: 2102 (m, Pt-C≡C), 2144 (m, C≡CSiMe$_3$) cm^{-1}. MS (MALDI-TOF) *m/z*: 1514.6 [M]$^+$. Anal. Calcd for $C_{86}H_{104}O_4P_2PtSi_2$: C, 68.18; H, 6.92. Found: C, 67.99; H, 6.85.

Synthesis of *trans*-Pt{C≡CC$_6$H$_2$(Ohex)$_2$C≡CSiMe$_3$}$_2$(PEt$_3$)$_2$ (1b)

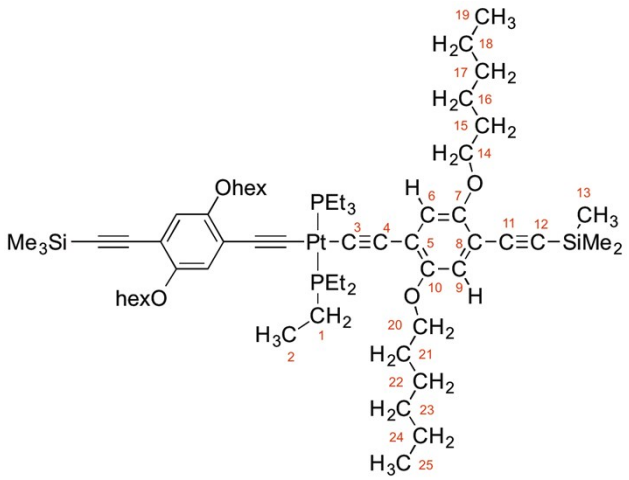

A mixture of *cis*-/*trans*-$PtCl_2(PEt_3)_2$ (1.00 g, 1.99 mmol) and copper iodide (5 mg, 0.03 mmol) was added to a solution of 2-trimethylsilylethynyl-5-ethynyl-1,4-bis(hexyloxy)benzene (2.00 g, 5.04 mmol) in dry triethylamine (40 ml) and the mixture heated to reflux under nitrogen for 48 hours. After cooling to room temperature, the solvent was removed *in vacuo* and the residue purified by column chromatography (silica, CH_2Cl_2/hexane, 1:1 v/v) to give the title compound as yellow powder after removal of the solvent from the main fraction (1.70 g, 70 %). ^{1}H NMR ($CDCl_3$, 500 MHz, δ / ppm): 0.24 (s, 18H, *13*), 0.87 – 0.93 (m, 12H, *19* and *25*), 1.15 – 1.24 (m, 18H, *2*), 1.29 – 1.37 (m, 16H, *17*, *18, 23,24*), 1.38 – 1.46 (m, 4H, *16* or *22*), 1.46 – 1.54 (m, 4H, *16* or *22*), 1.72 – 1.81 (m, 8H, *15, 21*), 2.17 – 2.26 (m, 12H, *1*), 3.90 (t, *J* = 6.9 Hz, 4H, *20*), 3.92 (t, *J* = 6.4 Hz, 4H, *14*) 6.77 (s, 2H, *9*), 6.80 (s, 2H, *6*). ^{13}C{^{1}H} NMR ($CDCl_3$, 125 MHz, δ / ppm): 0.2 (s, *13*), 8.5 (s, *2*), 14.21 (s, *19* or *25*), 14.24 (s, *19* or *25*), 16.4 (pseudo-t, apparent *J* = 17.4 Hz, *1*), 22.79 (s, *17* or *18* or *23* or *24*), 22.81 (s, *17* or *18* or *23* or *24*), 25.9 (br s, *16* and *22*), 29.58 (s, *15* or *21*), 29.62 (s, *15* or *21*), 31.83 (s, *17* or *18* or *23* or *24*), 31.86 (s, *17* or *18* or *23* or *24*), 69.2 (s, *14* or *20*), 69.8 (s, *14* or *20*), 98.2 (s, *12*), 102.4 (s, *4*, *5*, *8* or *11*), 105.7 (s, *4*, *5*, *8* or *11*), 110.1 (s, *4*, *5*, *8* or *11*), 115.5 (m, *3*), 116.5 (s, *6* or *9*), 118.3 (s, *6* or *9*), 120.1 (s, *4*, *5*, *8* or *11*), 153.2 (s, *7* or *10*), 154.3 (s, *7* or *10*). ^{31}P{^{1}H} NMR ($CDCl_3$, 202 MHz, δ / ppm): 11.7 (s, $J_{P\text{-}Pt}$ = 2364 Hz). IR (ATR) ν_{max}: 2095 (s, Pt-C≡C), 2150 (m, C≡CSiMe$_3$). MS (ESI-TOF) *m/z:* 453.1 [M-

H+Na]$^+$, 1249.7 [M+Na]$^+$. HRMS (ESI-TOF) *m/z:* [M+H]$^+$ calcd for $C_{62}H_{105}O_4P_2{}^{194}PtSi_2$ 1226.6675; found 1226.6689. Anal. Calcd for $C_{62}H_{104}O_4P_2PtSi_2$: C, 60.71; H, 8.55. Found: C, 60.57; H, 8.65.

Synthesis of *trans*-Pt{C≡CC_6H_4C≡C$SiMe_3$}$_2$(PPh_3)$_2$ (2a)

A solution of *cis*-$PtCl_2(PPh_3)_2$ (300 mg, 0.36 mmol), 1-ethynyl-4-trimethylsilylethynylbenzene (168 mg, 0.72 mmol) and copper iodide (6 mg, 0.03 mmol) in degassed diethylamine (30 ml) was heated at reflux for 3 hours. After this time, the resulting precipitate was collected by filtration and washed with MeOH to give the title compound as a pale yellow powder (340 mg, 85%). ^{1}H NMR ($CDCl_3$, 600 MHz, δ / ppm): 0.19 (s, 18H, Si*Me$_3$*), 6.17 (d, *J* = 8.3 Hz, 4H, Ar), 7.00 (d, *J* = 8.3 Hz, 4H, Ar), 7.29 - 7.36 (m, 16H, Ph_o), 7.36 – 7.42 (m, 8H, Ph_p), 7.74 – 7.80 (m, 16H, Ph_m). ^{13}C{^{1}H} NMR ($CDCl_3$, 151 MHz, δ / ppm): 0.2 (s, $SiMe_3$), 94.1 (s, *C*-$SiMe_3$), 106.0 (s, *C*≡ or C_{Ar}), 114.1 (m, Pt-*C*≡), 118.9 (s, *C*≡ or C_{Ar}), 128.0 (pseudo-t, apparent *J* = 5.5 Hz, Ph_m), 128.9 (s, *C*≡ or C_{Ar}), 129.2 (s, Ph_p), 130.4 (s, C_{Ar}), 130.7 (s, C_{Ar}-H), 130.9 (s, C_{Ar}-H), 131.3 (pseudo-t, apparent *J* = 29.3 Hz, Ph_i), 135.2 (m, Ph_o). ^{31}P{^{1}H} NMR ($CDCl_3$, 243 MHz, δ / ppm): 16.8 (s, $J_{P\text{-}Pt}$ = 2627 Hz). IR (CH_2Cl_2) ν_{max}: 2104 (m, Pt-C≡C), 2150 (m, C≡C$SiMe_3$) cm^{-1}. MS (MALDI-TOF) *m/z*: 718.9 [Pt$(PPh_3)_2$]$^+$, 1114.2 [M + H]$^+$, 1957.3. HRMS (ESI-TOF) *m/z:* [M+Na]$^+$ calcd for $C_{62}H_{56}P_2{}^{195}PtSi_2K$ 1152.2681; found 1152.2684. Anal. Calcd for $C_{62}H_{56}P_2PtSi_2$: C, 66.83; H, 5.07. Found: C, 67.00; H, 5.11. Crystals suitable for X-ray study were obtained from CH_2Cl_2/MeOH.

Synthesis of *trans*-Pt{C≡CC$_6$H$_4$C≡CSiMe$_3$}$_2$(PEt$_3$)$_2$ (2b)

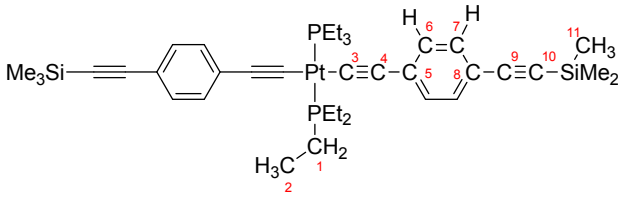

A mixture of *cis-/trans*-$PtCl_2(PEt_3)_2$ (200 mg, 0.40 mmol) and copper iodide (5 mg, 0.03 mmol) was added to a solution of 1-ethynyl-4-trimethylsilylethynylbenzene (198 mg, 1.00 mmol) in dry triethylamine (15 ml) and the obtained mixture heated to reflux under nitrogen for 48 hours. After allowing the solution to cool, the solvent was removed *in vacuo* and the residue purified by column chromatography (silica, CH_2Cl_2 : hexane 1:1 v/v). The crude product was recrystallised from CH_2Cl_2/hexane (143 mg, 44%). ^{1}H NMR ($CDCl_3$, 600 MHz, δ / ppm): 0.24 (s, 18H, *11*), 1.16 - 1.26 (m, 18H, *2*), 2.11 - 2.22 (m, 12H, *1*), 7.17 (d, *J* = 8.1 Hz, 4H, *6* or *7*), 7.30 (d, *J* = 7.9 Hz, 4H, *6* or *7*). ^{13}C{^{1}H} NMR ($CDCl_3$, 151 MHz, δ / ppm): 0.2 (s, *11*), 8.5 (s, *2*), 16.5 (pseudo-t, apparent, *J* = 17.5 Hz, *1*), 94.5 (s, *10*), 105.8 (s, *4*, *5*, *8* or *9*), 109.9 (s, *4*, *5*, *8* or *9*), 111.3 (m, *3*), 119.5 (s, *4*, *5*, *8* or *9*), 129.2 (s, *4*, *5*, *8* or *9*), 130.8 (s, *6* or *7*), 131.8 (s, *6* or *7*). ^{31}P{^{1}H}NMR ($CDCl_3$, 243 MHz, δ / ppm): 11.1 (s, $J_{P\text{-}Pt}$ = 2368 Hz). IR (ATR) ν_{max}: 2098 (s, Pt-C≡C), 2153 (m, C≡CSiMe$_3$) cm^{-1}. MS (ESI-TOF) *m/z:* 453.1 [Pt(PEt$_3$)$_2$-H+Na]$^+$, 826.3[M+H]$^+$. HRMS (ESI-TOF) *m/z:* [M+H]$^+$ calcd for $C_{38}H_{57}P_2{}^{195}PtSi_2$ 826.3106; found 826.3122. Anal. Calcd for $C_{38}H_{56}P_2PtSi_2$: C, 55.25; H, 6.83. Found: C, 55.18; H, 6.77. Crystals suitable for X-ray structure determination were obtained from toluene/ethanol.

Synthesis of *trans*-Pt(C≡CC≡CSiMe$_3$)$_2$(PPh$_3$)$_2$ (3a)[10]

A suspension of *cis*-$PtCl_2(PPh_3)_2$ (79 mg, 0.10 mmol), 1-trimethylsilylbuta-1,3-diyne (61 mg, 0.08 ml) and copper iodide (6 mg, 0.03 mmol) in CH_2Cl_2 (5 ml) and diethylamine (15 ml) was stirred at room temperature for 3 hours and then heated at 80 °C for a further 2 hours. The solvent was removed from

the resulting brown solution and the residue was purified by column chromatography (neutral alumina, toluene). The main fraction was collected concentrated and treated with MeOH to give the title compound as an off-white colored precipitate that was collected by filtration and dried in air (45 mg, 47%). ^{1}H NMR ($CDCl_3$, 400 MHz, δ / ppm): 0.01 (s, 18H, Si*Me*$_3$), 7.39 - 7.41 (m, 18H, Ph), 7.65 - 7.70 (m, 12H, Ph). ^{31}P {H} NMR ($CDCl_3$, 162 MHz, δ / ppm): 17.4 (s, $J_{P\text{-}Pt}$ = 2572 Hz). IR (CH_2Cl_2) ν_{max}: 2129 (s, Pt-C≡C), 2186 (m, C≡CSiMe$_3$) cm^{-1}.

Synthesis of *trans*-Pt(C≡CC≡CSiMe$_3$)$_2$(PEt$_3$)$_2$ (3b)

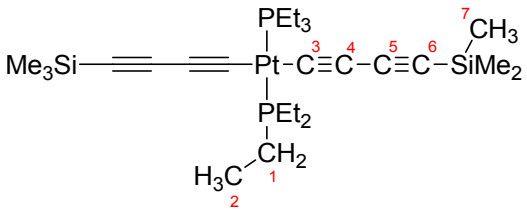

A mixture of *cis*-/*trans*-$PtCl_2(PEt_3)_2$ (200 mg, 0.40 mmol) and copper iodide (5 mg, 0.03 mmol) was added to a solution of 1-trimethylsilylbuta-1,3-diyne (122 mg, 1.00 mmol) in dry triethylamine (15 ml) and the reaction solution heated at reflux under a nitrogen atmosphere for 48 hours. After cooling to room temperature, the solvent was removed *in vacuo* and the residue purified by column chromatography (silica, CH_2Cl_2/hexane, 1:1 v/v). The product was obtained as a pale yellow powder after removal of the solvent from the main fraction (202 mg, 68 %). ^{1}H NMR ($CDCl_3$, 500 MHz, δ / ppm): 0.15 (s, 18H, *7*), 1.07 - 1.15 (m, 18H, *2*), 2.00 - 2.10 (m, 12H, *1*). ^{13}C{^{1}H} NMR ($CDCl_3$, 126 MHz, δ / ppm): 0.3 (s, *7*), 8.3 (s, *2*), 16.3 (pseudo-t, apparent *J* = 17.5 Hz, *1*), 76.7 (s, *6*), 92.2 (m, *4* or *5*), 92.3 (m, *4* or *5*), 102.6 (m, *3*). ^{31}P{^{1}H} NMR ($CDCl_3$, 151 MHz, δ / ppm): 12.8 (s, $J_{P\text{-}Pt}$ = 2306 Hz). IR (ATR) ν_{max}: 2128 (s, Pt-C≡C), 2185 (m, sh (2173), C≡CSiMe$_3$) cm^{-1}. MS (ESI-TOF) *m/z:* 453.1 [Pt(PEt$_3$)$_2$-H+Na]$^+$, 674.2 [M+H]$^+$, 696.2 [M+Na]$^+$, 712.2 [M+K]$^+$, 728.3 [M+Na+MeOH]$^+$, 738.3

$[M+H+2MeOH]^+$, 1347.5 $[2M+H]^+$. HRMS (ESI-TOF) *m/z:* $[M+H]^+$ calcd for $C_{26}H_{49}P_2{}^{195}PtSi_2$ 674.2498; found 674.2496. Anal. Calcd for $C_{26}H_{48}P_2PtSi_2$: C, 46.34; H, 7.18. Found: C, 46.18; H, 7.03.

Synthesis of *trans*-Pt(C≡CC$_6$H$_4$Bu^t-4)$_2$(PPh$_3$)$_2$ (4a)

A mixture of *cis*-$PtCl_2(PPh_3)_2$ (100 mg, 0.13 mmol), 4-*tert*-butylphenylacetylene (45 mg, 0.05 ml, 0.28 mmol) and copper iodide (2 mg, 0.01 mmol) in diisopropylamine (10 ml) was stirred at room temperature overnight. The solution was filtered and the precipitate was washed with MeOH and dried to give an off-white solid (92 mg, 69%). ^{1}H NMR ($CDCl_3$, 500 MHz, δ / ppm): 1.19 (s, 18H, C*H*$_3$), 6.20 (d, *J* = 8.0 Hz, 4H, Ar), 6.92 (d, *J* = 8.0 Hz, 4H, Ar), 7.33 - 7.37 (m, 12H, Ph), 7.38 - 7.42 (m, 6H, Ph), 7.78 - 7.84 (m, 12H, Ph). ^{13}C {^{1}H} NMR ($CDCl_3$, 126 MHz, δ / ppm): 31.4 (s, *C*H$_3$), 34.5 (s, C_{tBu}), 109.5 (m, Pt-*C*≡), 113.2 (s, *C*≡ or C_{Ar}), 124.1 (s, C_{Ar}-H), 125.9 (s, *C*≡ or C_{Ar}) 127.9 (m, Ph_m), 130.2 (s, C_{Ar}-H), 130.7 (s, Ph_p), 131.8 (m, Ph_i), 135.3 (m, Ph_o), 147.4 (s, C_{Ar}-CMe$_3$). ^{31}P {^{1}H} NMR ($CDCl_3$, 202 MHz, δ / ppm): 18.6 (s, $J_{P\text{-}Pt}$ = 2662 Hz). IR (CH_2Cl_2) ν_{max}: (Pt-C≡C) 2108 cm^{-1}. MS (MALDI-TOF) *m/z*: 719.1 $[Pt(PPh_3)_2]^+$, 1033.3 $[M]^+$. HRMS (ESI-TOF) *m/z:* $[M+Na]^+$ calcd for $C_{60}H_{56}P_2{}^{195}PtNa$ 1056.3403; found 1056.3429.

Synthesis of *trans*-Pt(C≡CC$_6$H$_4$Bu^t-4)$_2$(PEt$_3$)$_2$ (4b)

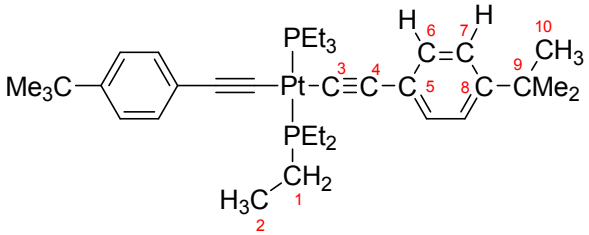

A mixture of *cis*-/*trans*-$PtCl_2(PEt_3)_2$ (250 mg, 0.50 mmol) and copper iodide (5 mg, 0.03 mmol) was added to a solution of 4-*tert*-butylphenylacetylene (198 mg, 1.25 mmol) in dry triethylamine (15 ml) and

the reaction solution heated at reflux under nitrogen for 48 hours. After cooling to room temperature, the solvent was removed *in vacuo* and the residue purified by column chromatography (silica, CH_2Cl_2/hexane, 1:1 v/v). The crude product was obtained from the main fraction and recrystallised from CH_2Cl_2/MeOH (342 mg, 89 %). ^{1}H NMR ($CDCl_3$, 600 MHz, δ / ppm): 1.17 - 1.25 (m, 18H, *2*), 1.29 (s, 18H, *10*), 2.12 - 2.21 (m, 12H, *1*), 7.20 - 7.25 (m, 8H, *6* and *7*). ^{13}C{^{1}H} NMR ($CDCl_3$, 151 MHz, δ / ppm): 8.5 (s, *2*), 16.4 (pseudo-t, apparent J = 17.5 Hz, *1*), 31.4 (s, *10*), 34.6 (s, *9*), 106.5 (m, *3*), 109.3 (s, *4*), 125.0 (s, *6* or *7*), 126.2 (s, *5*), 130.6 (s, *6* or *7*), 147.9 (s, *8*). ^{31}P{^{1}H} NMR ($CDCl_3$, 243 MHz, δ / ppm): 10.9 (s, $J_{P\text{-}Pt}$ = 2386 Hz), IR (ATR) ν_{max}: 2103 (s, Pt-C≡C) cm^{-1}. HRMS (ESI-TOF) *m/z:* 453.1 $[Pt(PEt_3)_2\text{-H+Na}]^+$, 746.4 $[M+H]^+$, 768.3 $[M+Na]^+$, 784.3 $[M+K]^+$, 800.4 $[M+Na+MeOH]^+$, 809.4 $[M+2MeOH]^+$. HRMS (ESI-TOF) *m/z:* $[M+H]^+$ calcd for $C_{36}H_{57}P_2{}^{195}Pt$ 746.3593; found 746.3583. Anal. Calcd for $C_{36}H_{56}P_2Pt$: C, 57.97; H, 7.57. Found: C, 57.89; H, 7.69.

Crystal structure determinations

Data were measured from single crystals using an Oxford Diffraction Gemini-R Ultra CCD diffractometer with monochromatic MoKα radiation (λ = 0.71073 Å). Data were corrected for Lorentz and polarization effects and absorption correction applied. The structures were solved by direct method and refined by full-matrix least-squares on F^2 using the SHELX crystallographic package.[11] Non-hydrogen atoms were refined anisotropically using all reflections. The positions of hydrogen atoms were calculated and their atomic parameters were constrained to the bonded atoms during the refinement.

Crystal/refinement details for ***2a****:* $C_{62}H_{56}P_2PtSi_2$, M = 1114.27, light-yellow prism, 0.29 x□0.11 x□0.09 mm^3, orthorhombic, space group *Pbcn* (No. 60), a = 21.2751(3), b = 13.91150(17), c = 18.2617(2) Å,□V = 5404.88(12) Å^3, Z = 4, D_c = 1.369 g/cm^3,□□□ = 2.737 mm^{-1}. F_{000} = 2256, T = 120(2) K, 2□$_{max}$ = 61.9º, 62222 reflections collected, 7526 unique (R_{int} = 0.0533). Final *GooF* = 1.027, *R1* = 0.0272, *wR2* = 0.0586, R indices based on 5042 reflections with I > 2□ (I), |□□|$_{max}$= 0.84(8) e Å^{-3}, 307 parameters, 0 restraints. CCDC reference: 1513125

Crystal/refinement details for ***2b****:* $C_{38}H_{56}P_2PtSi_2$, M = 826.04, colorless plate, 0.27 x□0.20 x□0.05 mm^3, triclinic, space group *P***Error!** (No. 2), a = 11.4323(3), b = 11.8869(3), c = 14.4775(4) Å,□ □ = 90.438(2),□□□ = 93.368(2),□□□ = 92.628(2)°, V = 1961.84(9) Å^3, Z = 2, D_c = 1.398 g/cm^3,□□□ = 3.743 mm^{-1}. F_{000} = 840, T = 100(2) K, 2□$_{max}$ = 64.6º, 41642 reflections collected, 12993 unique (R_{int} = 0.0458). Final *GooF* = 1.002, *R1* = 0.0309, *wR2* = 0.0683, R indices based on 9708 reflections with I > 2□ (I), |□□|$_{max}$= 1.4(1) e Å^{-3}, 403 parameters, 0 restraints. CCDC reference: 1513126

Single-molecule conductance measurements

Acetone cleaning and flame-annealing was used to prepare gold on glass substrates (Arrandee, Schröer, Germany). Flame-annealing was achieved with a butane torch used to heat the samples to a slight orange glow, with the slide being kept in this state for about 20 seconds with constant motion being used to prevent avoid overheating. This flame-annealing procedure was performed 3 times to yield Au (111) terraced samples.[12] These freshly prepared substrates were then immersed in a 10^{-4} M acetonitrile (99.9% ChromasolV Plus for HPLC) solution of the complex under investigation for 1 minute. The gold sample was then removed and rinsed with ethanol and then dried in a gaseous flow of argon.

The *I*(*s*) method was used to determine conductance values of the complexes and their break off-distances. For these measurements an STM (Agilent 5500 SPM microscope), was used with an electrochemically etched gold tip. This STM tip is approached close to the gold substrate surface and then rapidly retracted while simultaneously recording the tunneling (*I*) as a function of the retraction distance (*s*).[13] STM set point conditions of $I = 30$ nA and bias voltage, $Utip = 0.6$ V were employed and the instrument was fitted with a low-current preamplifier to optimize signal measurement. The retraction and approach of the STM tip is repeated many times in a cyclic manner, each time starting from the aforementioned set-point values. Molecular junctions occasionally form during these cycles and these manifest themselves as deviations from the usual exponential decay of the tunneling current with retraction distance. In such cases of molecular junction formation rather characteristic plateaus arise from the flow of tunneling current along the molecular backbone. These plateaus cease as the tip is retracted beyond the maximal stretching length of the molecule junction, with the current only then decaying to the zero baseline. This "non-contact" technique for creating molecular junctions generally results in a relatively low probability for forming molecular junctions, when compared to break junction techniques where there is initial metal-to-metal contact of the electrodes. Traces where molecular junctions form are called "molecular junction formation scans" and these are recognized by recording only traces which exhibit junction stretching lengths (or plateaus) longer than 1 Å. Given the relatively

low junction formation probability, the STM tip retraction cycles are repeated many times (~15000 traces) in order to record sufficient traces for statistical analysis. The junction formation probability was ~3.5% for the TMSE end groups. This very low junction formation probability for the TMSE terminal groups may be related to either their relatively weak contact binding or possibly their propensity to bind as only specific surface defects sites (e.g. gold steps) with sufficient conductance.[14] The resulting current-distance curves are binned in conductance steps of 16 pS and then plotted to give a conductance histogram comprised of at least 500 current-distance scans showing discernable plateaus. The error in each conductance value reported has been statistically obtained from the standard deviation of the points comprising a Gaussian line fit to the conductance peak. Representative $I(s)$ traces and 2D conductance plots are shown in Figures S1 – S8. The initial set-point distance of the tip from the surface S_0 is determined as described previously.[15] It should be recognised that the determination of S_0 is an approximation which is based on the determination of $d\ln(I)/ds$ (values shown in Table below), and an extrapolation back to the G_0 value to get the S_0 distance value, with the assumption that this slope value is linear over the extrapolation. If $d\ln(I)/ds$ values are underestimated then this will lead to an overestimation of the S_0 value and the junction breaking distances.

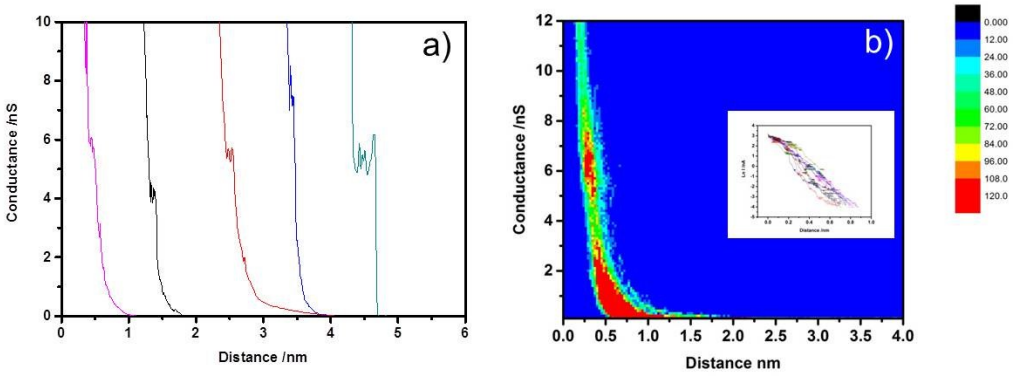

Figures S1: a) I(s) scans of molecule **2a**. **b)** 2D histogram without the S_0 value added to the distance value. Inset typical ln *I(s)* scans used for the calibration of S_0.

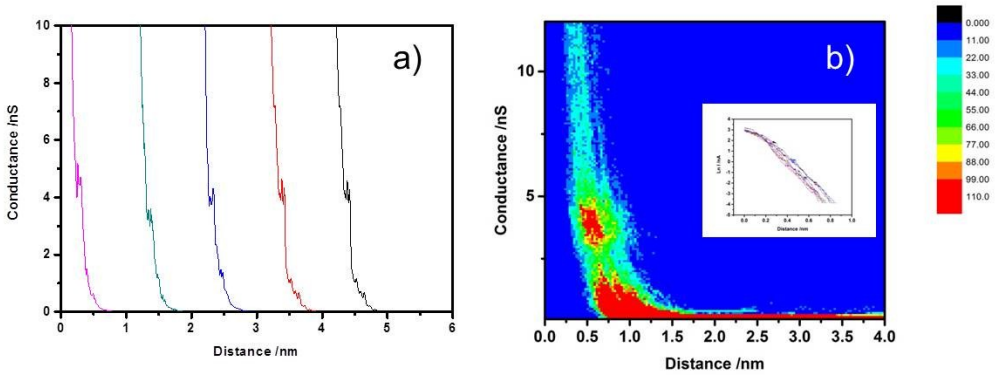

Figures S2: a) I(s) scans of molecule **3a**. **b)** 2D histogram without the S_0 value added to the distance value. Inset typical ln *I(s)* scans used for the calibration of S_0.

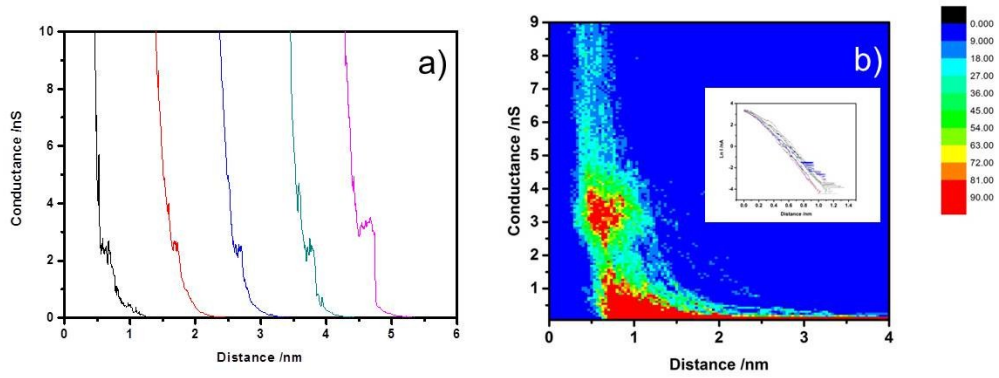

Figures S3: a) I(s) scans of molecule **4a**. **b)** 2D histogram without the S_0 value added to the distance value. Inset typical ln *I(s)* scans used for the calibration of S_0.

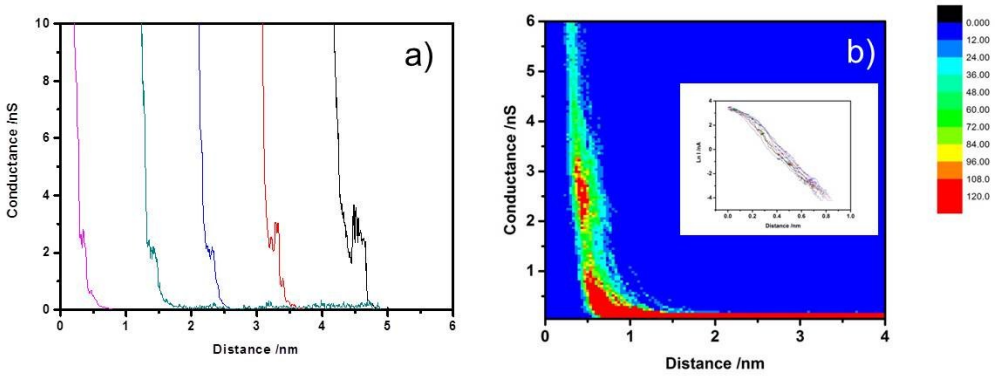

Figures S4: a) I(s) scans of molecule **1a**. **b)** 2D histogram without the S_0 value added to the distance value. Inset typical ln *I(s)* scans used for the calibration of S_0.

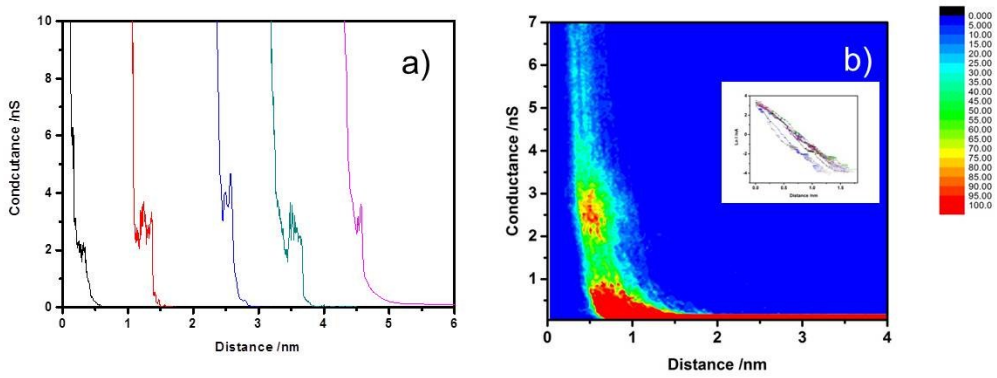

Figures S5: a) I(s) scans of molecule **1b**. **b)** 2D histogram without the S_0 value added to the distance value. Inset typical ln *I(s)* scans used for the calibration of S_0.

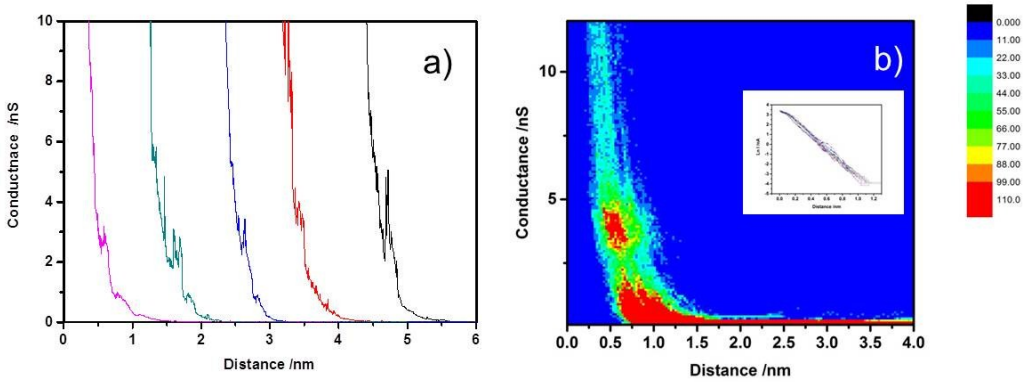

Figures S6: a) I(s) scans of molecule **3b**. **b)** 2D histogram without the S_0 value added to the distance value. Inset typical ln *I(s)* scans used for the calibration of S_0.

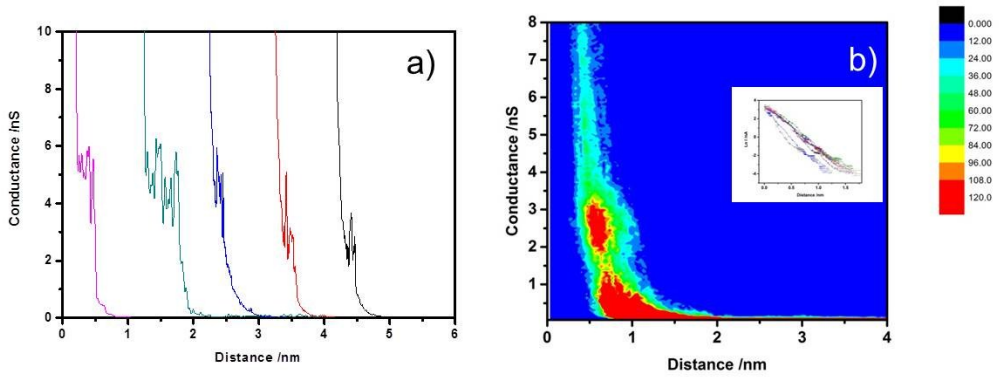

Figures S7: a) I(s) scans of molecule **2b**. **b)** 2D histogram without the S_0 value added to the distance value. Inset typical ln *I(s)* scans used for the calibration of S_0.

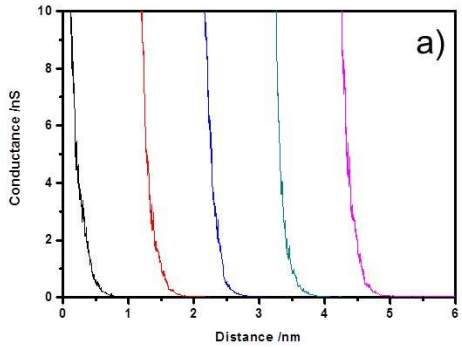

Figures S8: a) I(s) scans of molecule **4b**.

Molecule	S_0 nm	dln(*I*)/d*s*
1a	1.4	5.2
1b	1.4	5.3
2a	1.4	5.1
2b	1.1	6.5
3a	1.0	7.3
3b	1.4	5.2
4a	0.8	9.4

Theoretical methods

Gas-phase geometry optimizations were performed with the Gaussian 09 program package,[16] using the B3LYP functional[17,18] and LANL2DZ basis set on Ru and Pt[19-21] and 6-31G** on all other atoms.[22] Electronic structures were explored using GaussSum. [23]

The DFT-Landauer approach used in the modelling assumes that on the timescale taken by an electron to traverse the molecule, inelastic scattering is negligible. This is known to be an accurate assumption for molecules up to several nm in length.[24] Geometrical optimizations were carried out using the DFT code SIESTA,[25] with a generalized gradient approximation (PBE functional), double-ζ polarized basis set, 0.01 eV/A force tolerance and a real-space grid with a plane wave cut-off energy of 250 Ry, zero bias voltage and 1 k points.

To compute the electrical conductance of the molecules, eight layers of (111)-oriented bulk gold with each layer consisting of 6×6 atoms and a layer spacing of 0.235 nm were used to create the molecular junctions as shown in Figure 2, and described in detail elsewhere. [26,27] These layers were then further repeated to yield infinitely-long current-carrying gold electrodes. Each molecule was attached to two (111) directed gold electrodes; one of these electrodes is pyramidal, representing the STM tip, while the other is a planar slab representing the electrode formed by the idealized Au(111) substrate in the *I*(*s*) based molecular junction. The molecules and first layers of gold atoms within each electrode were then allowed to relax again, to yield the optimal junction geometries shown in Figure 2. From these model junctions the transmission coefficient, $T(E)$, was calculated using the GOLLUM code.[26] The room temperature electrical conductance G was computed for a range of Fermi energies E_F, and a single common value of E_F which gave the closest overall agreement with the experimental results was chosen. This yielded a value of $E_F - E_F^{DFT} = -0.4$ eV, which is used in all theoretical results presented in this manuscript. This is a commonly accepted procedure in molecular electronics DFT-based calculations. [28,29]

For each structure, the transmission coefficient *T(E)* describing the propagation of electrons of energy *E* from the left to the right electrode was calculated by first obtaining the corresponding Hamiltonian and overlap matrices using SIESTA and then using the GOLLUM code to compute *T(E)* via the relation

$$T(E) = \mathrm{Tr}\left\{\Gamma_R(E)G^R(E)\Gamma_L(E)G^{R\dagger}(E)\right\},$$

in this expression, $\Gamma_{L,R}(E) = i\left(\Sigma_{L,R}(E) - \Sigma_{L,R}{}^{\dagger}(E)\right)$ describes the level broadening due to the coupling between left (L) and right (R) electrodes and the central scattering region, $\Sigma_{L,R}(E)$ are the retarded self-energies associated with this coupling and $G^R = (ES - H - \Sigma_L - \Sigma_R)^{-1}$ is the retarded Green's function, where H is the Hamiltonian and S is the overlap matrix (both of them obtained from SIESTA). Finally the room temperature electrical conductance G was computed from the formula $G = G_0 \int_{-\infty}^{\infty} dE T(E)\left(-\frac{df(E)}{dE}\right)$ where $f(E) = [e^{\beta(E-E_F)} + 1]^{-1}$ is the Fermi function, $\beta = 1/k_B T$, E_F is the Fermi energy and $G_0 = \left(\frac{2e^2}{h}\right)$ is the quantum of conductance. Since the quantity $\left(-\frac{df(E)}{dE}\right)$ is a probability distribution peaked at $E=E_F$, with a width of the order k_BT, the above expression shows that G/G_0 is obtained by averaging T(E) over an energy range of order k_BT in the vicinity of $E=E_F$.

The use of DFT to compute the ground state energy of various molecular junctions permits the calculation of binding energies and optimal geometries. However, these calculations are subject to errors, due to the use of localized basis sets, which are concentrated on the nuclei. Therefore, we used the counterpoise method to obtain accurate energies.[30] This involves calculating: (a) the total DFT energies for the system ((Molecule plus gold (E_S)); (b) the energy of the isolated molecule in the same conformation adopted in the presence of gold electrode (E_M); (c) the energy of the system in the absence of the molecule (E_G). For each of these energy calculations, we used the same basis functions as those described for the complete junction models. With these data we calculated the binding energies E_b according to the expression $E_b = (E_S - E_M - E_G)$, [30,31] which are given in Table S2.

To confirm the concept that the higher values measured for **2a, 3a** and **4a** can be attributed to the binding of the molecule in the junction through the PPh_3 ligands, DFT-calculations have been performed for three different models of molecular junctions (Figure S9). The molecules in model **A** (Figure S9; first column) are contacted to the electrodes via ostensibly ancillary PPh_3 ligands and trimethylsilylethynyl moieties. The *trans*-PPh_3 ligands are attached to both electrodes in model **B** (Figure S9; second column). The third model **C** features trimethylsilylethynyl moieties contacted to both electrodes (Figure S9; third column).

Binding energies (Table S2) were calculated from (a) the total DFT energies for the system ((Molecule plus gold (E_S)); (b) the energy of the isolated molecule in the same conformation adopted in the presence of the gold electrode (E_M); (c) the energy of the system in the absence of the molecule (E_G). For each of these energy calculations, we used the same basis functions as those described for the complete junction models. With these data we calculated the binding energies E_b according to the expression $E_b = (E_S - E_M - E_G)$.[30,31] Binding energy results are shown in Table S2.

Figure S10 and Table S1 show that the calculated conductances as a function of Fermi energy for molecular junctions **2a**, **3a** and **4a** in three different models. The conductance of junctions in model **B** are the highest, and, with the exception of **4a**, an order of magnitude higher than the experimental conductance; the theoretical electrode separations (Z) are much shorter than the break-off distances. In contrast, the calculated values of conductance and Z from of the molecular junctions in model **A** show a good agreement with the experimental data. The lowest conductances and longest theoretical electrode separations (Z) are presented by the junctions in model **C**, which are not in agreement with the experimental results.

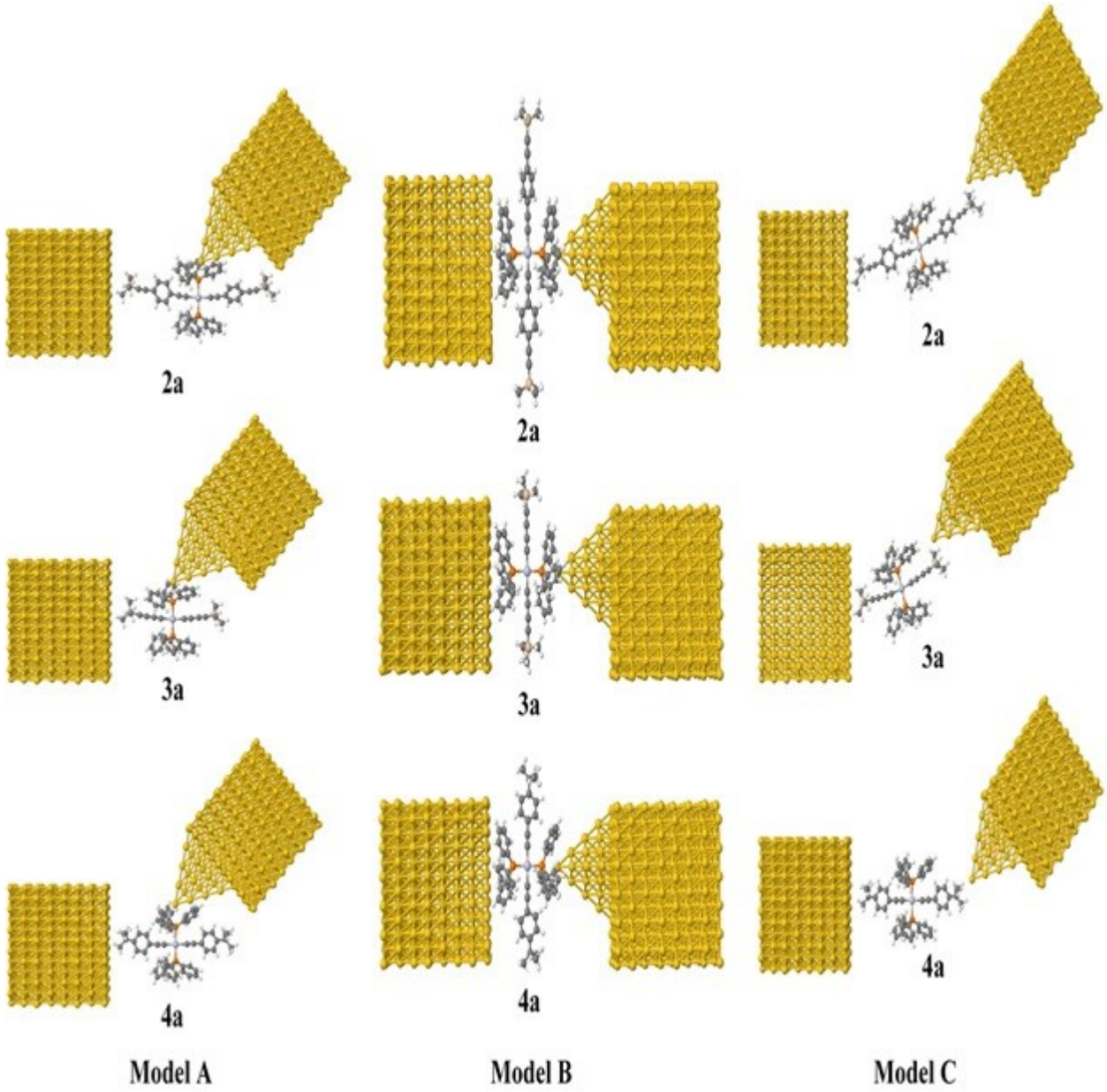

Figure S9. The relaxed geometries of molecular junctions **2a**, **3a**, and **4a** in three different models **(A, B** and **C)**.

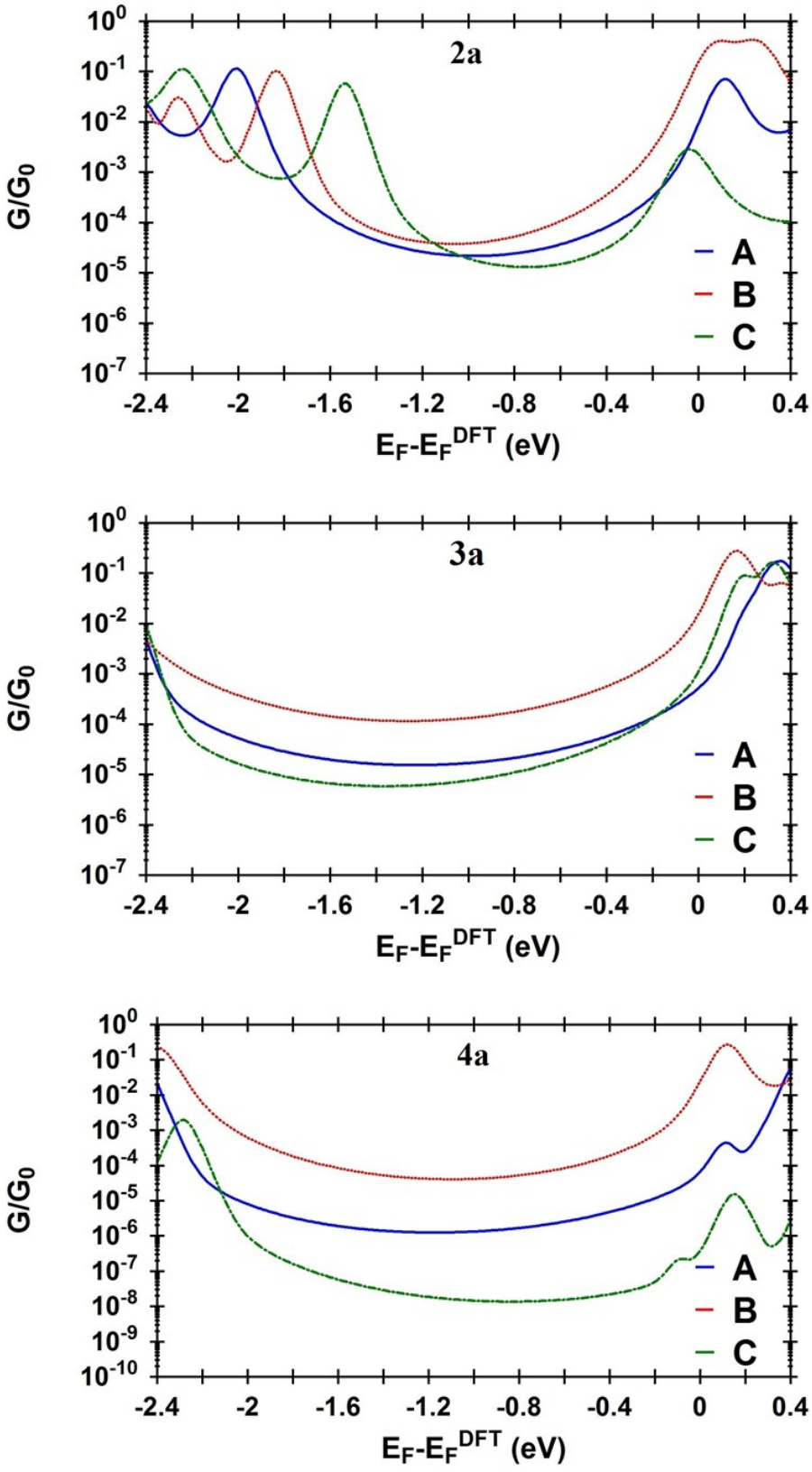

Figure S10. Plots showing comparisons of calculated conductance as a function of the Fermi energy for **2a**, **3a** and **4a** molecular junctions in three different models (**A**, **B** and **C**), as shown in figure S1.

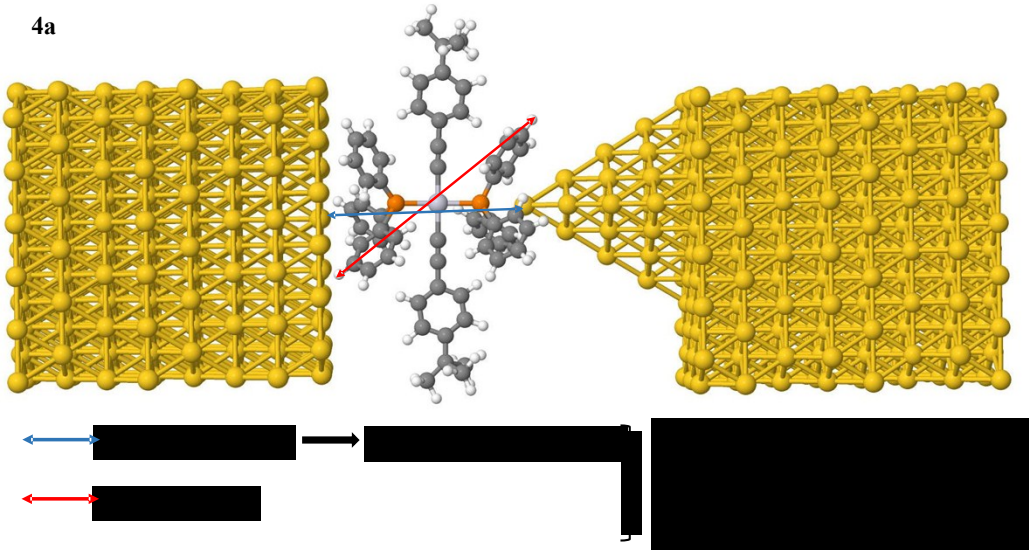

Figure S11. Geometrical distances in the Model A junction from **4a**.

Table S1. Summary of the conductance values and geometries from experimental and computational molecular junctions of three different models of molecular junctions (**A**, **B**, **C**). The expermental conductance (Exp. G/G_0) determined from $I(s)$ measurements. The calculated conductance values (Th. G/G_0) at $E_F - E_F^{DFT} = -0.4$ eV from the junction models. Experimental break-off distance (Z^*) from $I(s)$ measurments. The calculated electrode separation (Z) in a relaxed junction, $Z = d_{Au\text{-}Au} - 0.25$ nm, where 0.25 nm is the calculated center-to-center distance of the apex atoms of the two opposing gold electrodes when conductance = G_0 in the absence of a molecule.

Molecule	**Model A**		**Model B**		**Model C**		**Exp. G/G_0**	**Z^* (nm)**
	Th. G/G_0	**Z (nm)**	**Th. G/G_0**	**Z (nm)**	**Th. G/G_0**	**Z (nm)**		
2a	8×10^{-5}	1.73	3.44×10^{-4}	1.05	3.1×10^{-5}	2.33	$7.9\pm1.1\times10^{-5}$	1.70±0.1
3a	5.7×10^{-5}	1.37	5.66×10^{-4}	1.03	4.23×10^{-5}	1.72	$5.2\pm1.6\times10^{-5}$	1.38±0.1
4a	3.9×10^{-6}	1.69	1.98×10^{-5}	1.05	2.18×10^{-8}	2.25	$4.1\pm0.6\times10^{-5}$	1.46±0.21

Table S2. The calculated binding energies between **3a** and gold electrodes in model (B) with different distances (d) between the P atom of the molecule and the Au atom at the tip of the electrode.

Model	Binding Energy (eV)	d (nm)
B1	-3.46	0.20
B2	-1.93	0.25
B3	-1.01	0.30
B4	-0.38	0.35
B5	-0.12	0.40

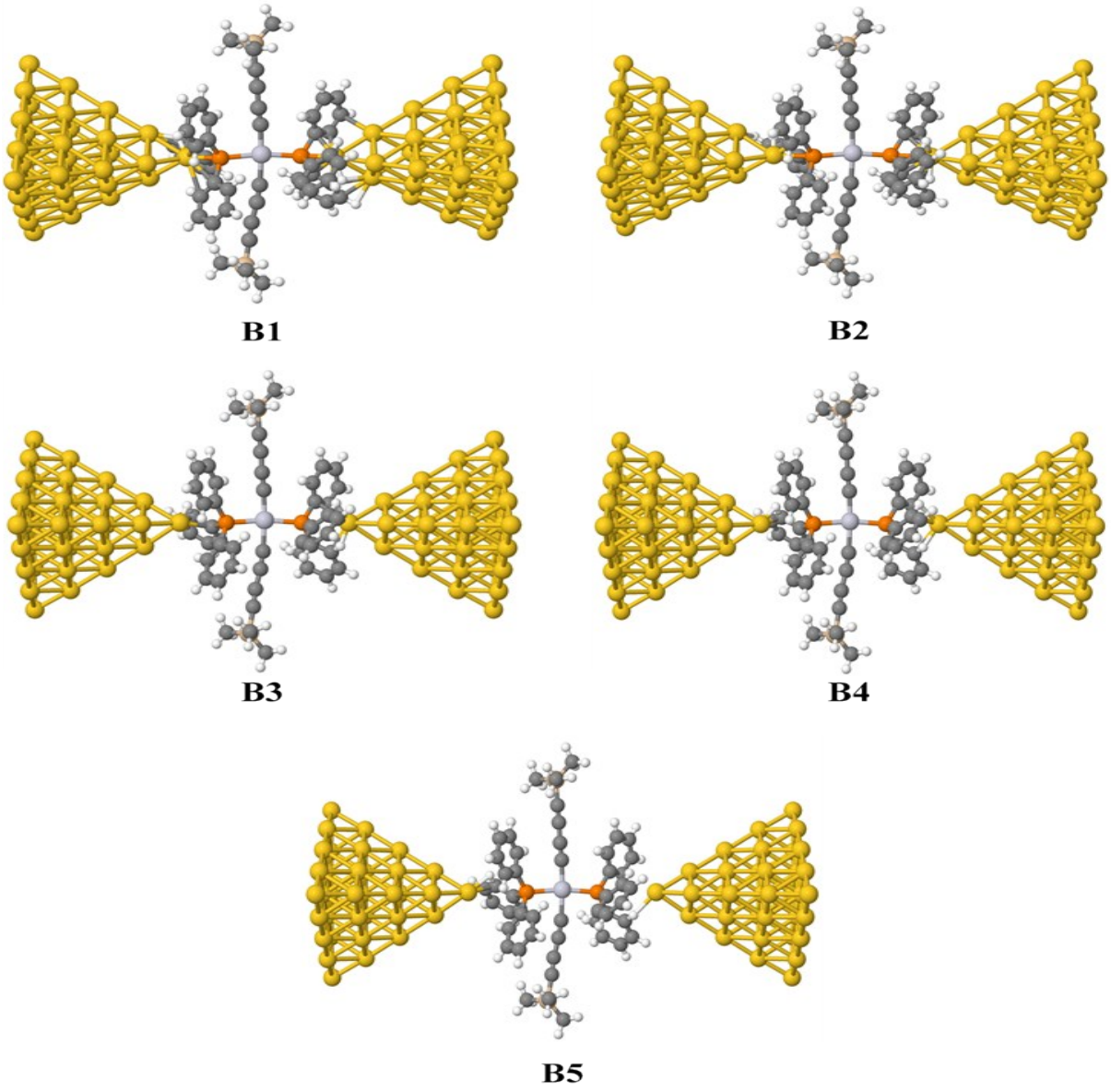

Figure S12. The geometries of molecular junctions (model B) formed from **3a** with different distances (d) between P atom of molecule and Au of the electrode.

NMR Spectra

trans-Pt{C≡CC_6H_2(Ohex)$_2$C≡C$SiMe_3$}$_2$(PPh_3)$_2$ (**1a**)

^{1}H NMR spectrum

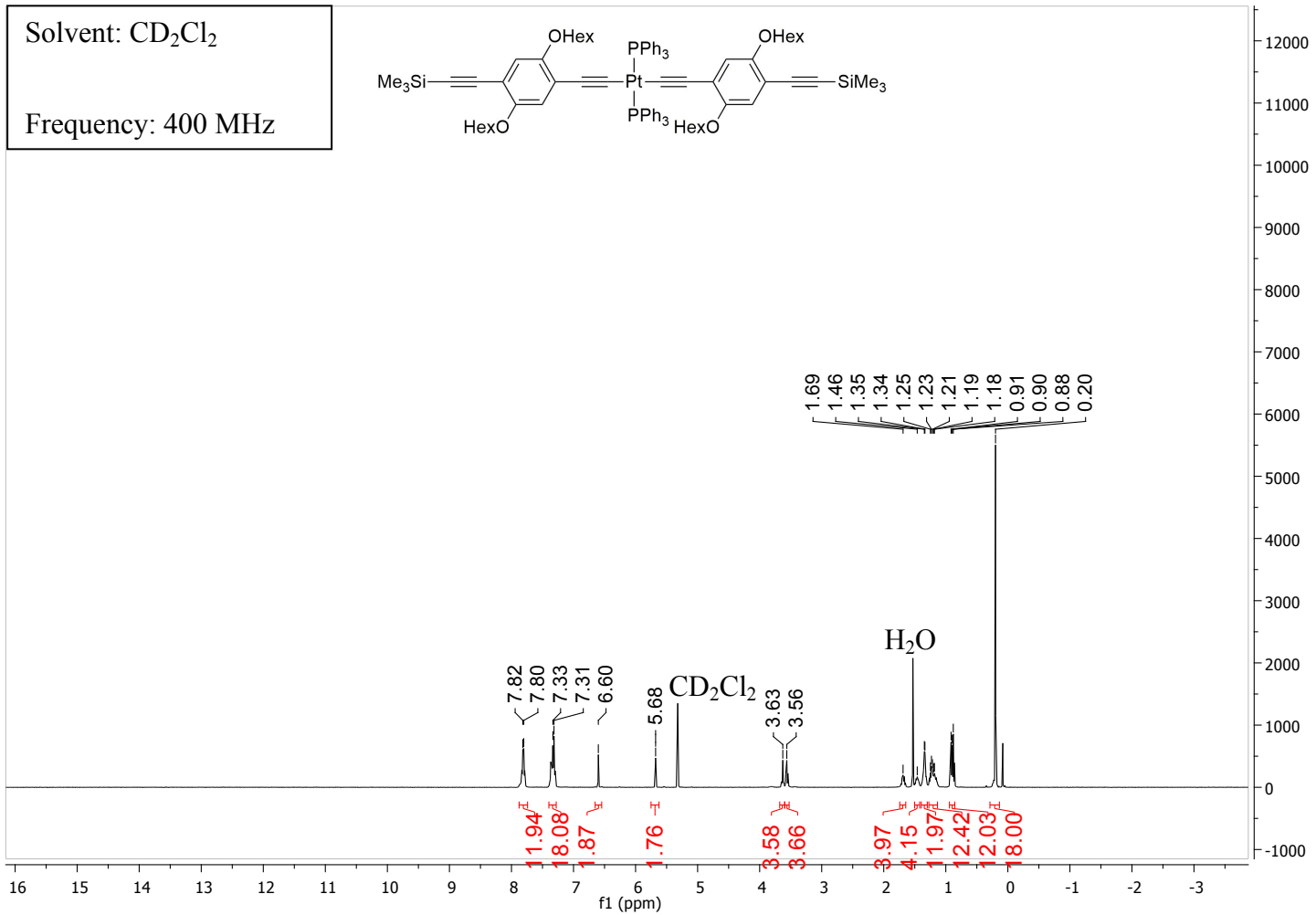

$^{31}P\{^{1}H\}$ NMR spectrum

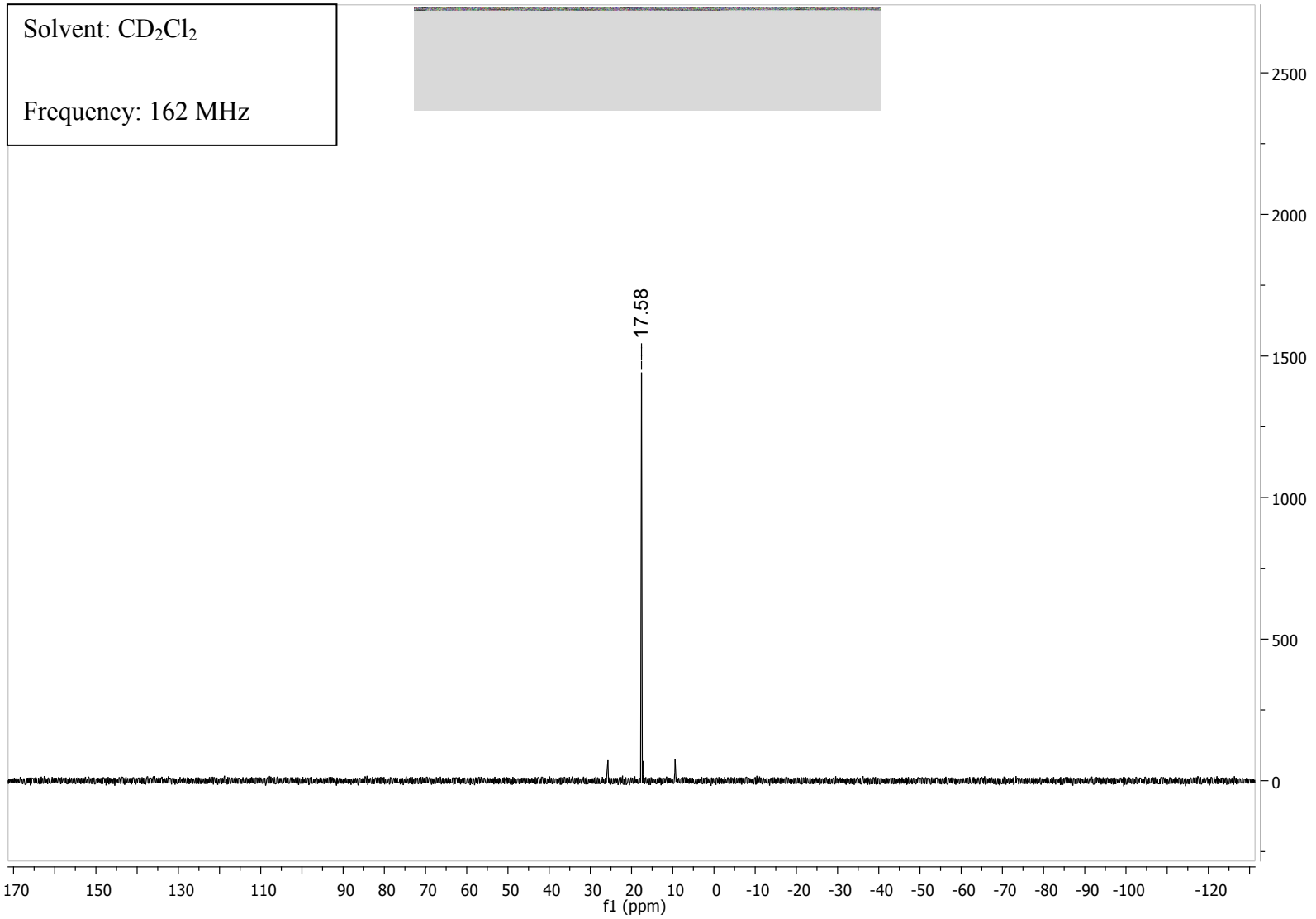

$^{13}C\{^{1}H\}$ NMR spectrum

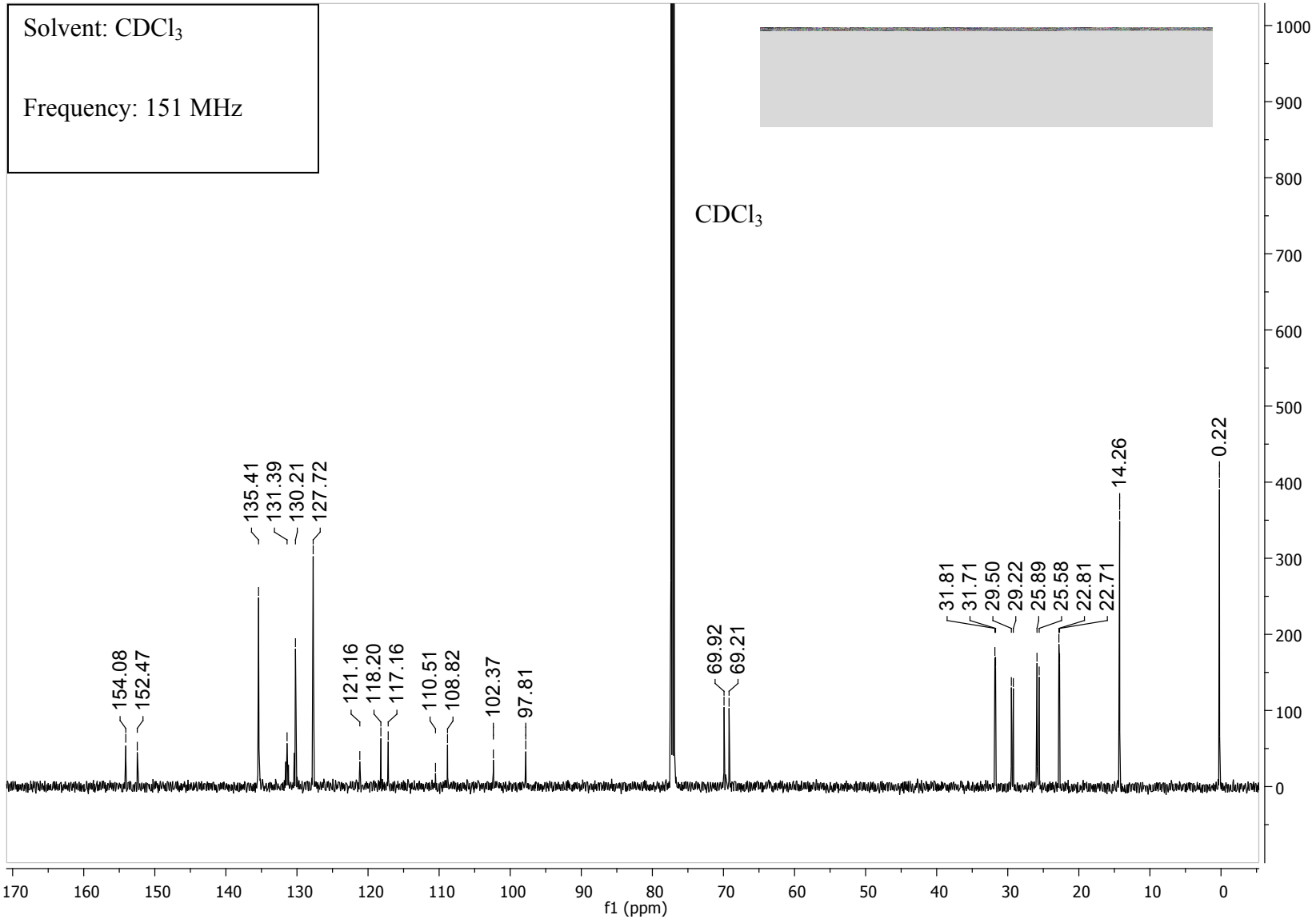

trans-Pt{C≡CC_6H_2(Ohex)$_2$C≡C$SiMe_3$}$_2$(PEt_3)$_2$ **(1b)**

^{1}H NMR spectrum

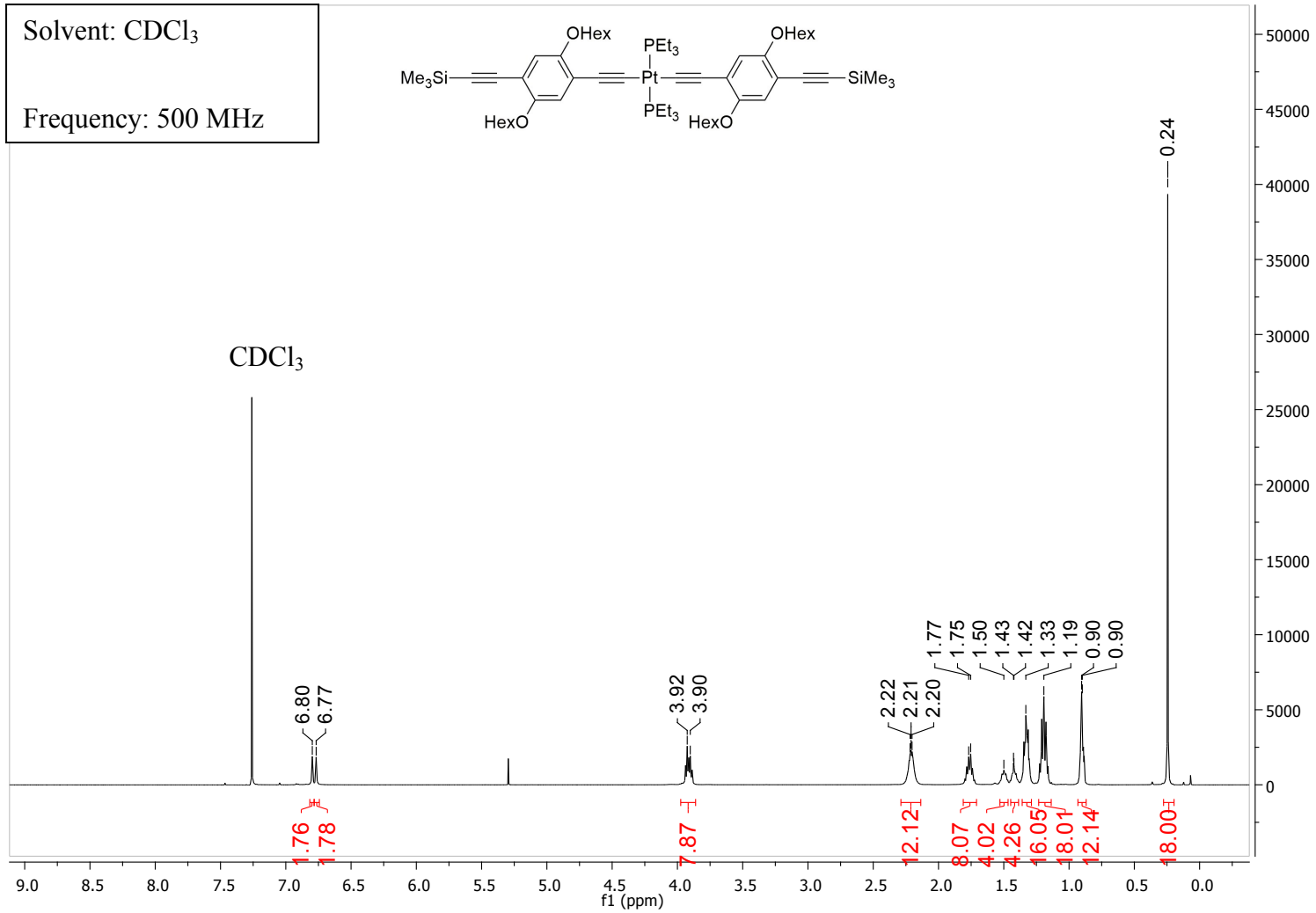

$^{31}P\{^{1}H\}$ NMR spectrum

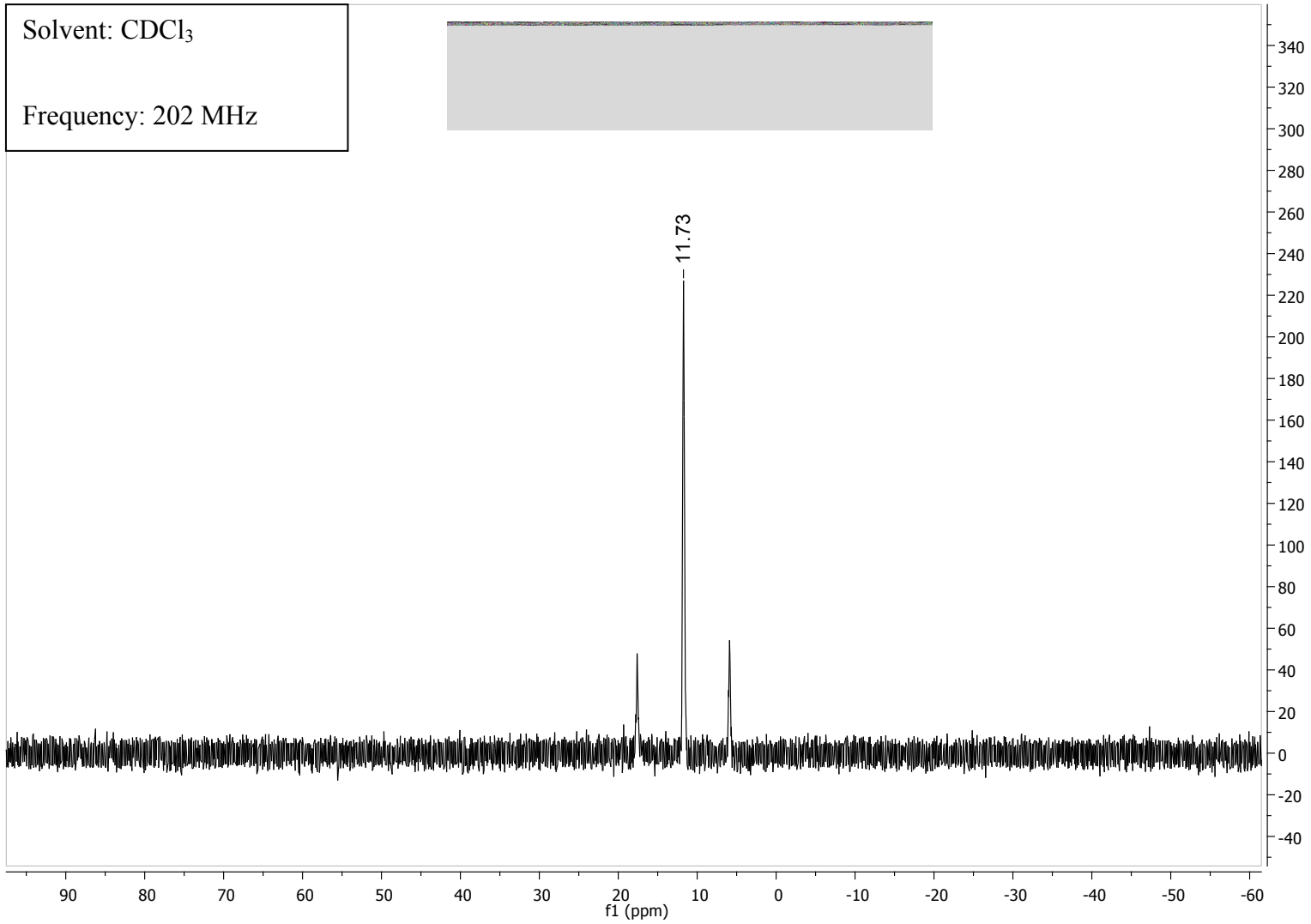

$^{13}C\{^{1}H\}$ NMR spectrum

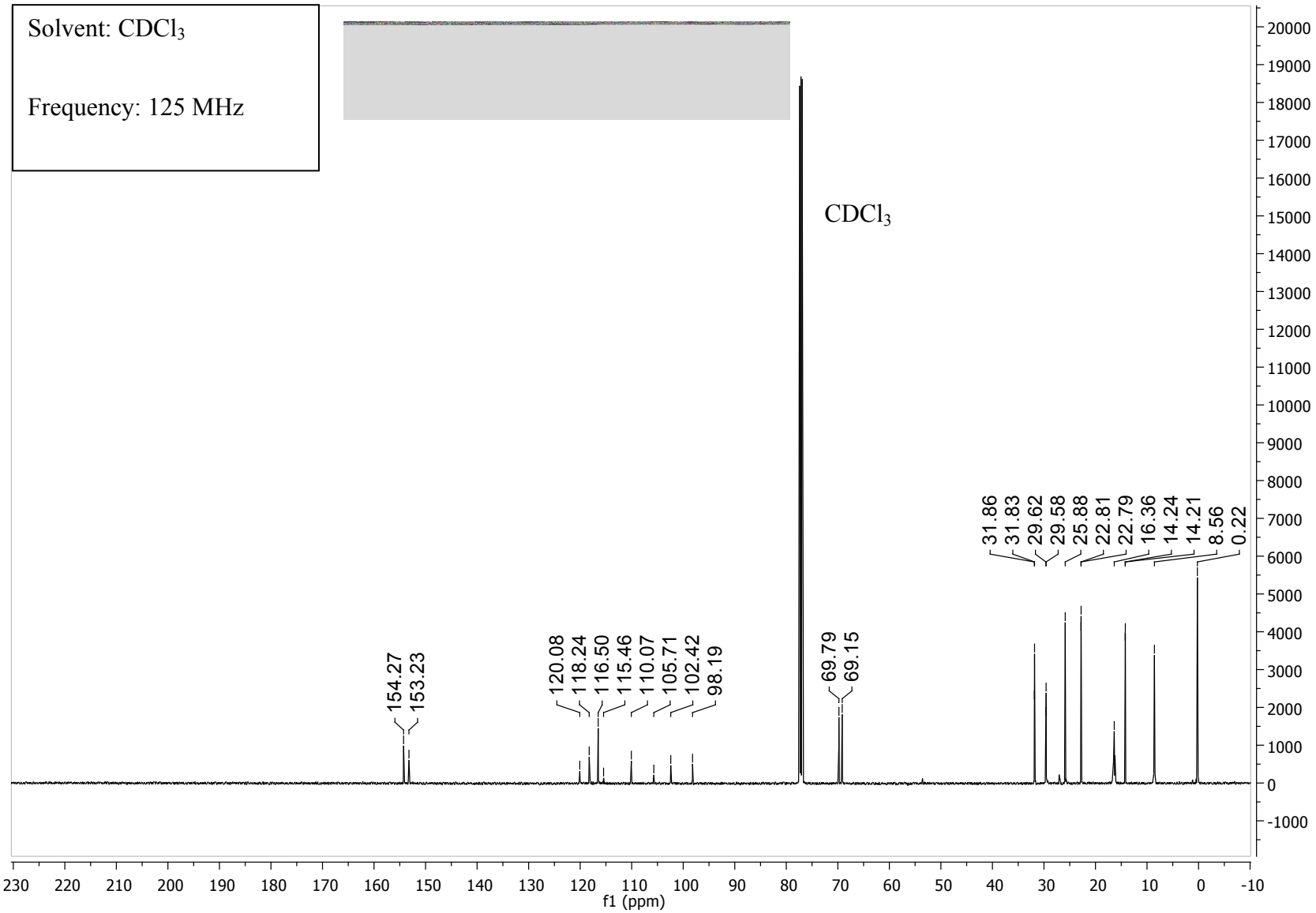

trans-Pt{C≡CC$_6$H$_4$C≡CSiMe$_3$}$_2$(PPh$_3$)$_2$ (**2a**)

^{1}H NMR spectrum

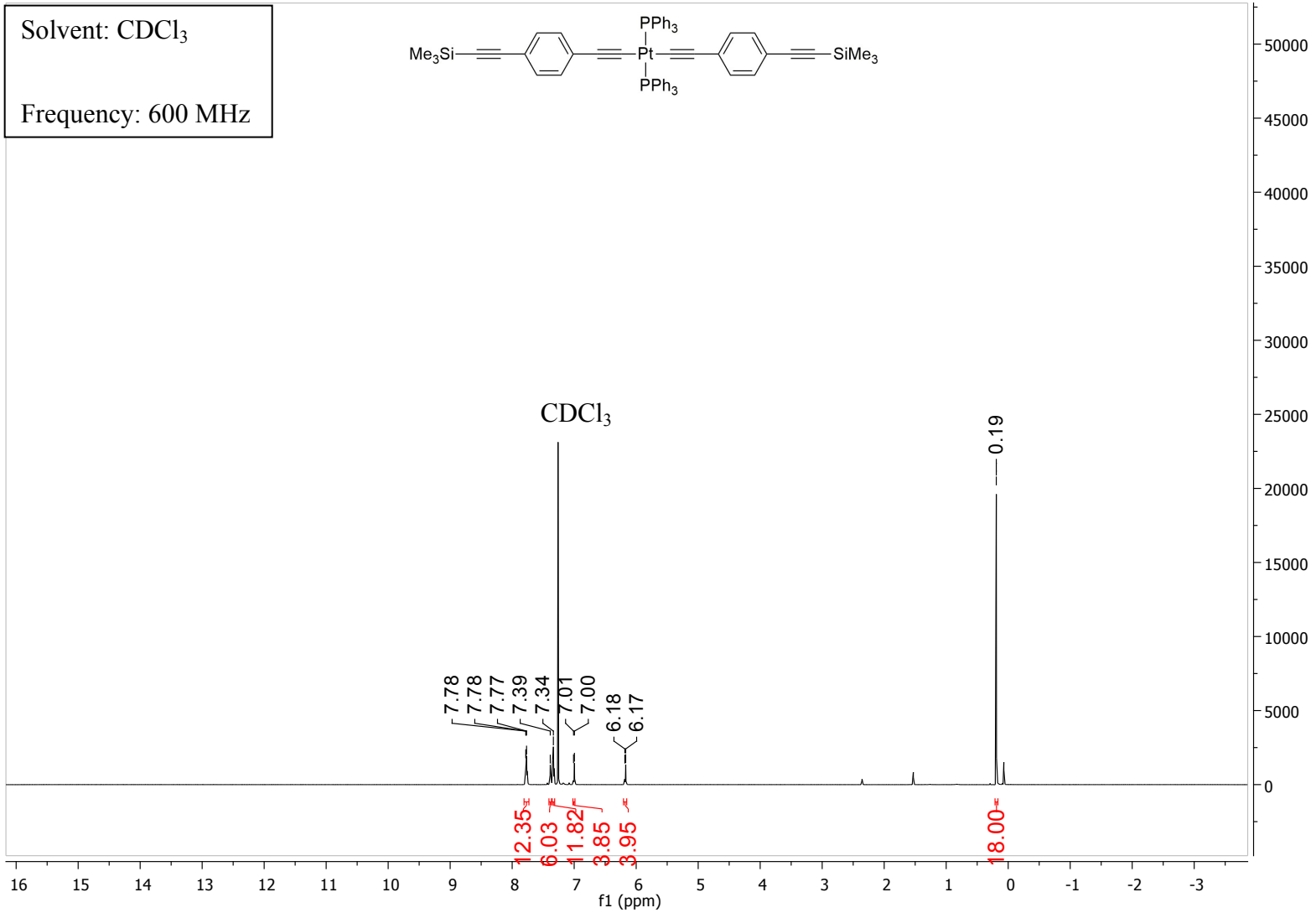

$^{31}P\{^{1}H\}$ NMR spectrum

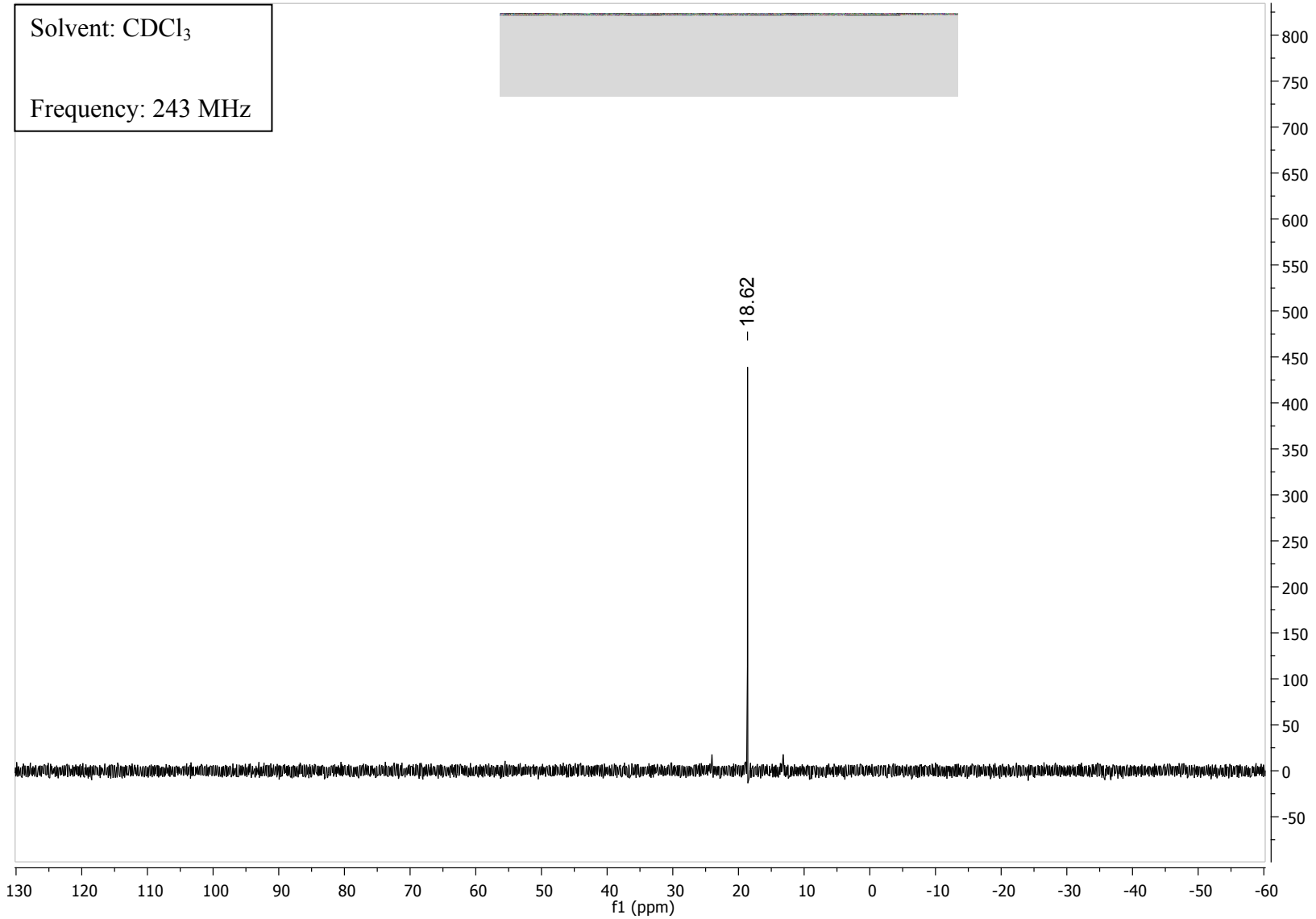

$^{13}C\{^{1}H\}$ NMR spectrum

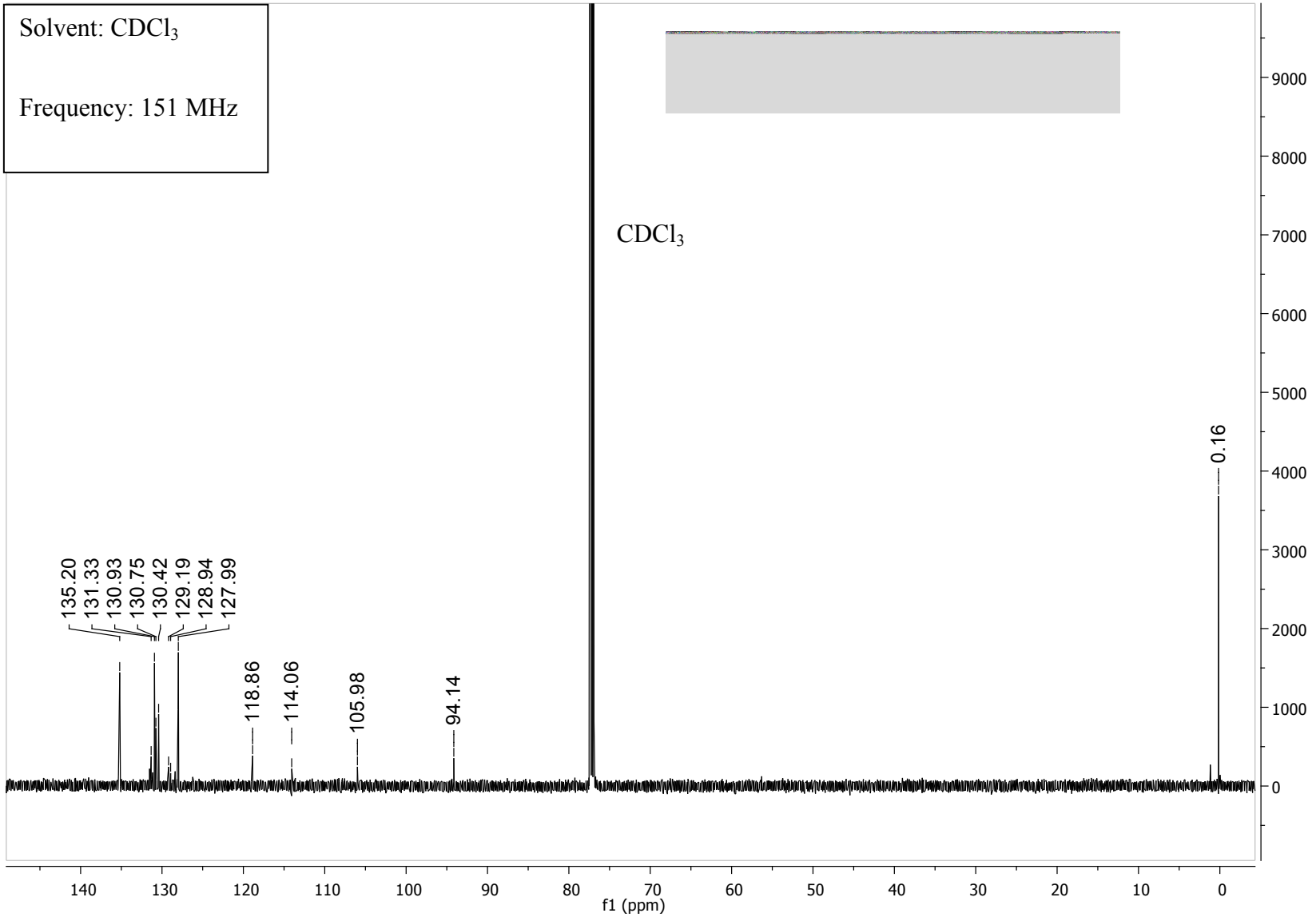

trans-Pt{C≡CC_6H_4C≡C$SiMe_3$}$_2$(PEt_3)$_2$ (**2b**)

^{1}H NMR spectrum

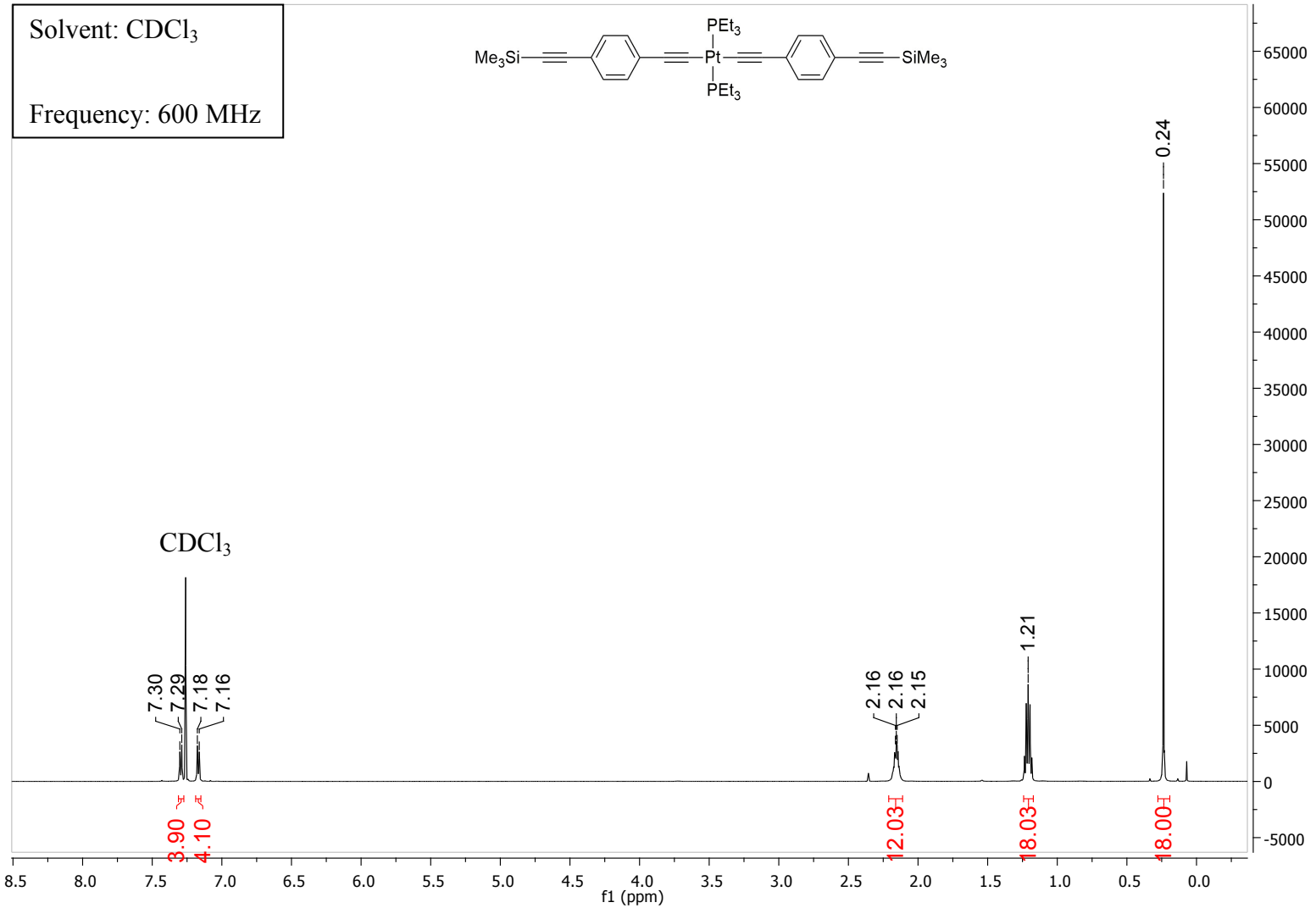

$^{31}P\{^{1}H\}$ NMR spectrum

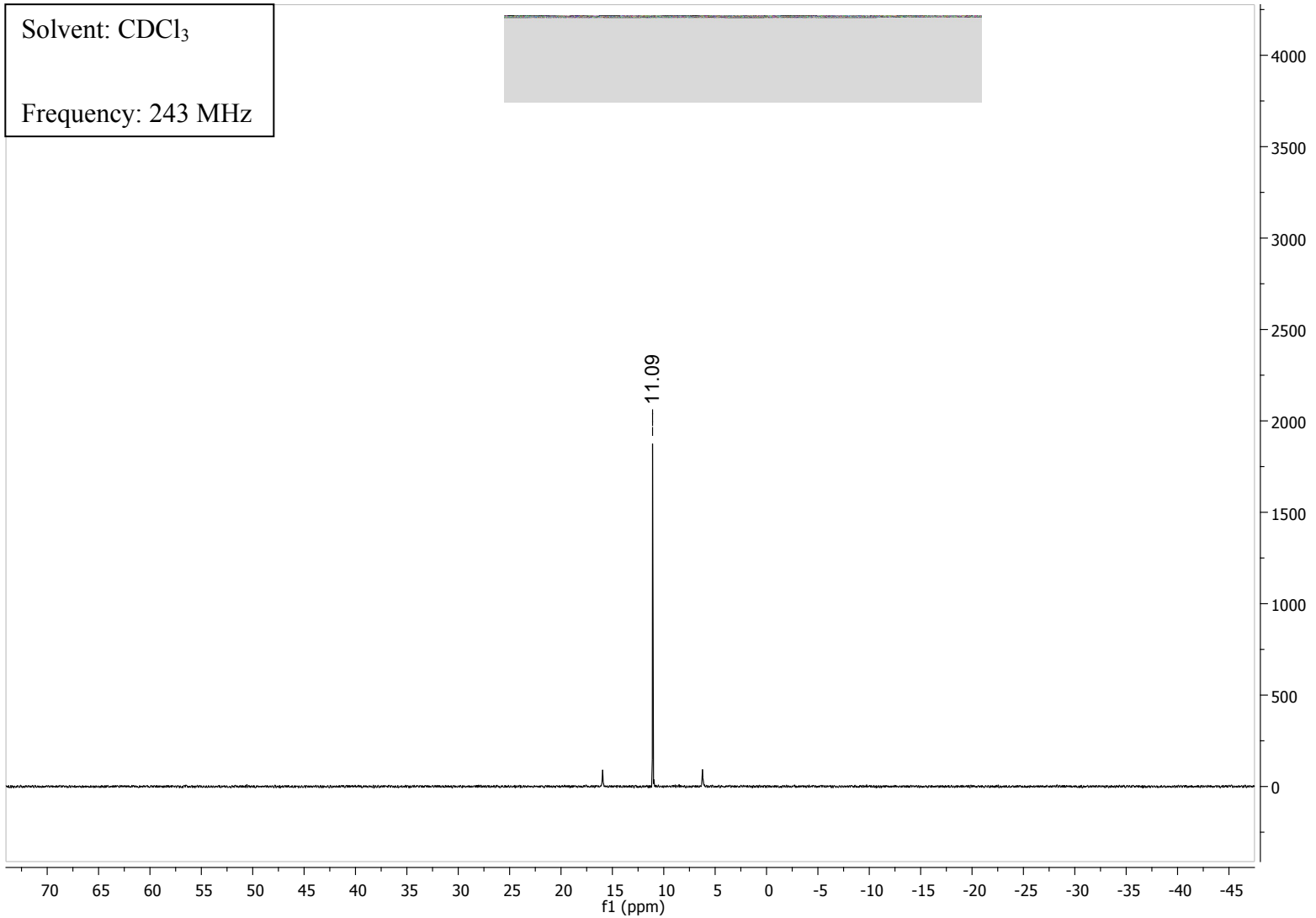

$^{13}C\{^{1}H\}$ NMR spectrum

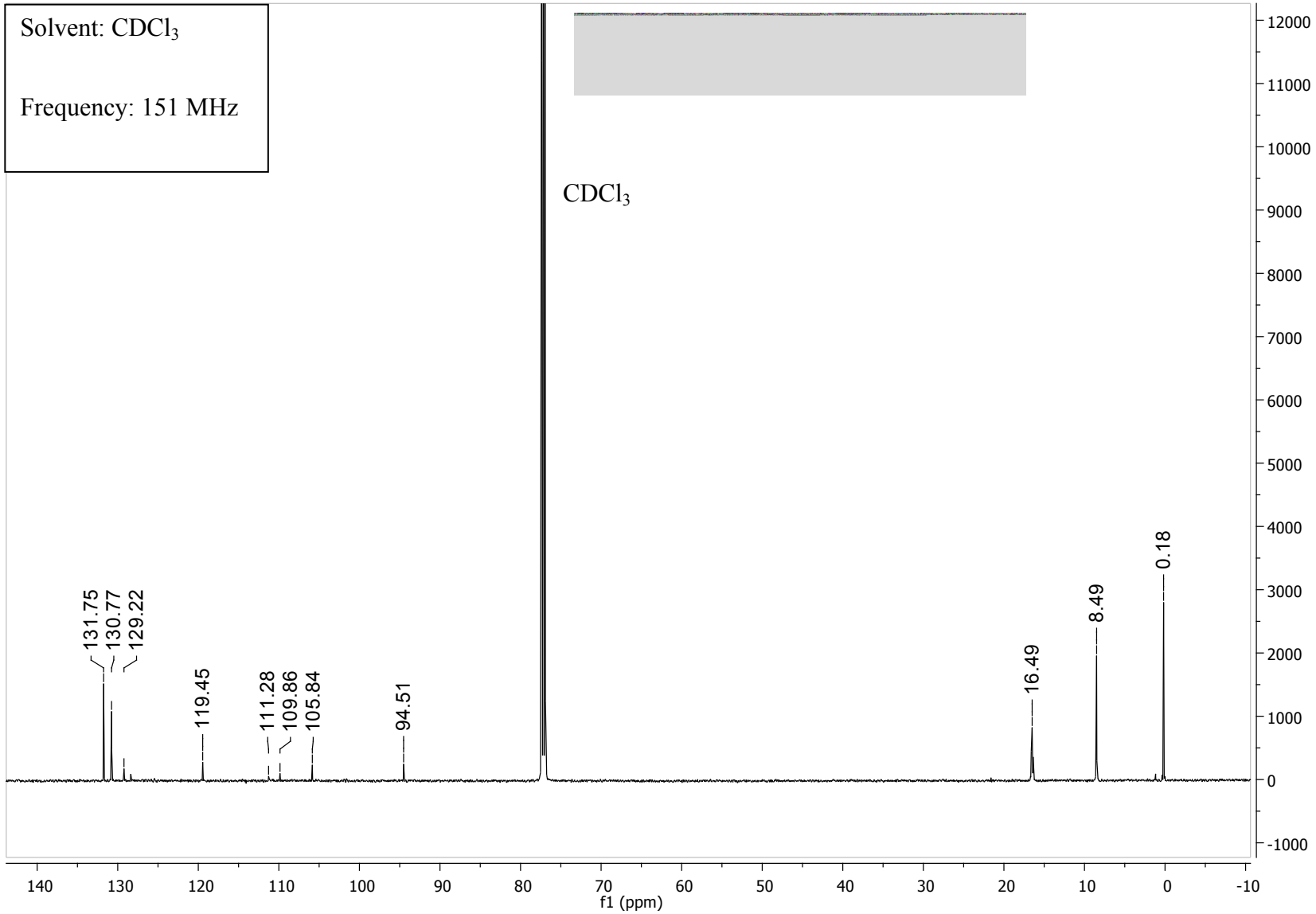

trans-Pt{C≡C-C≡CSiMe$_3$}$_2$(PEt$_3$)$_2$ **(3b)**

^{1}H NMR spectrum

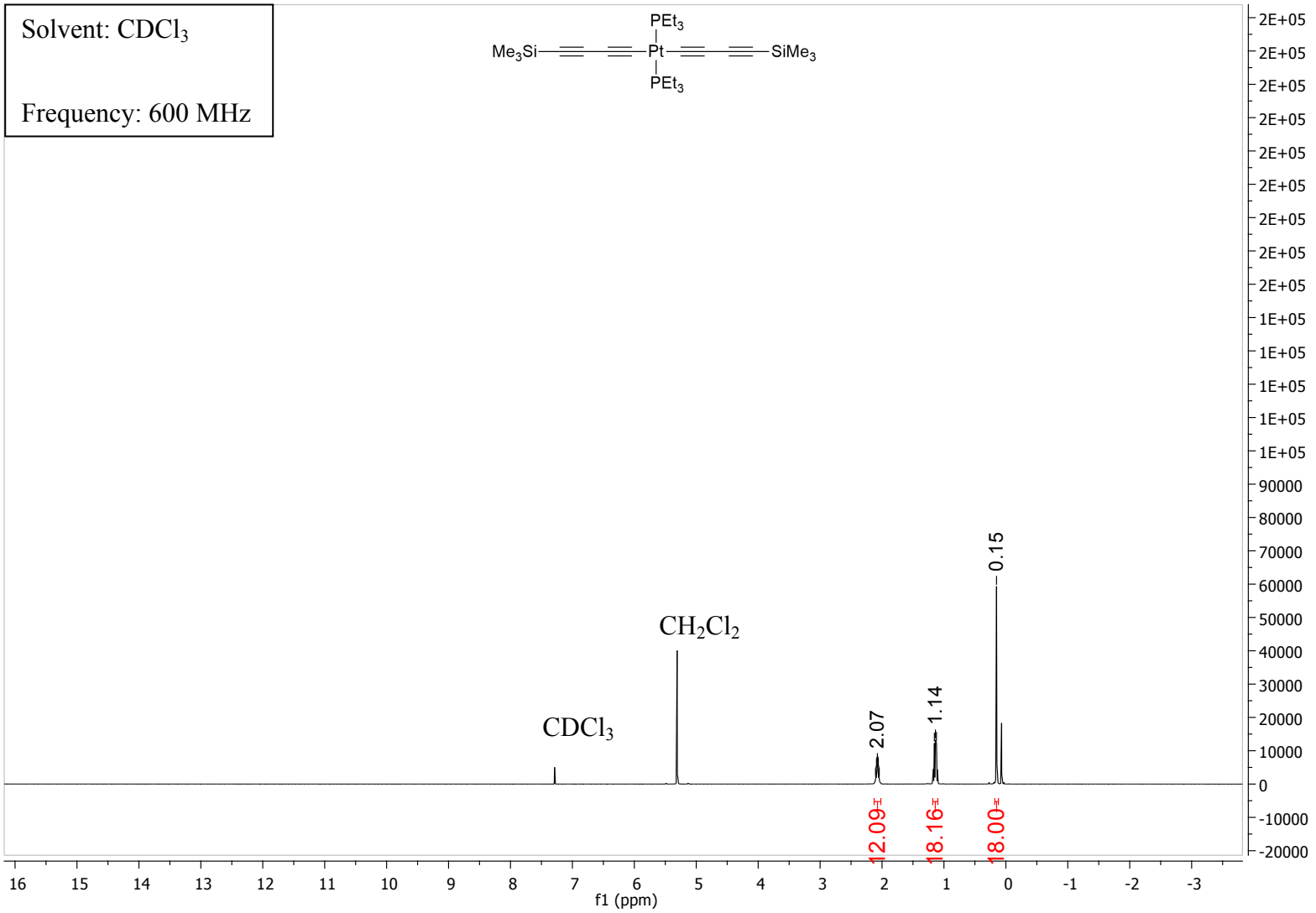

$^{31}P\{^{1}H\}$ NMR spectrum

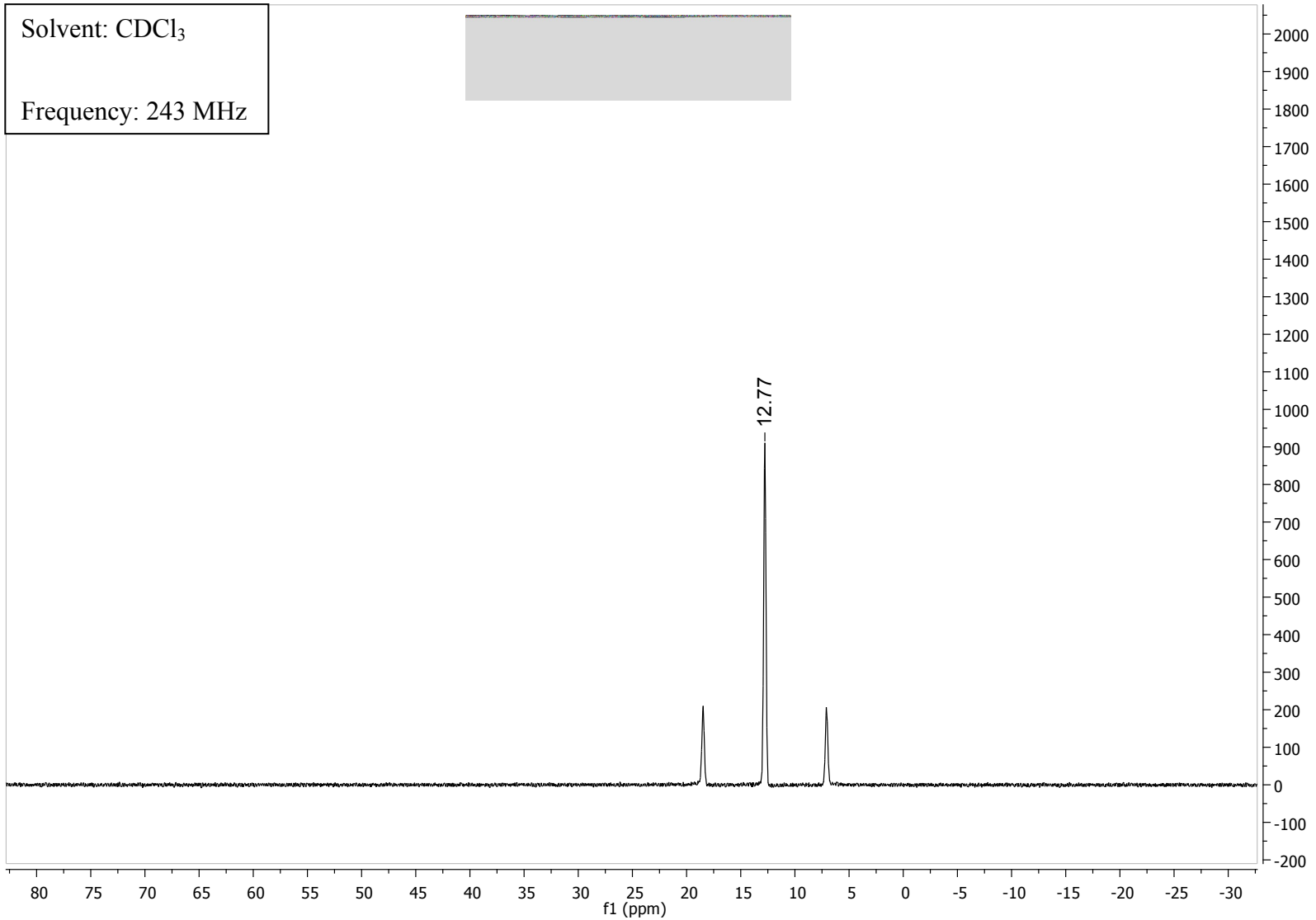

$^{13}C\{^{1}H\}$ NMR spectrum

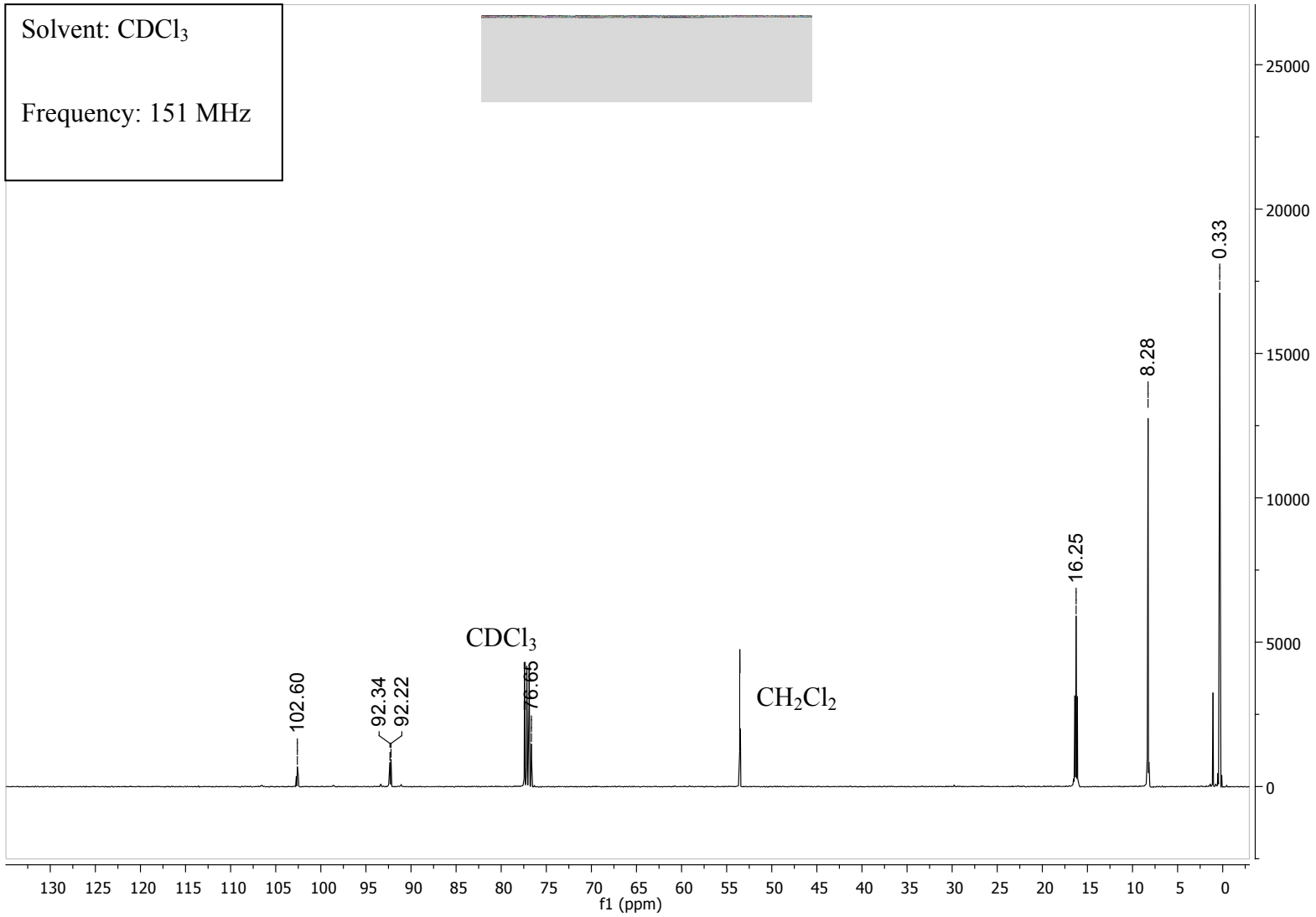

trans-Pt{C≡C-C_6H_4-CMe_3}$_2$(PPh_3)$_2$ (**4a**)

^{1}H NMR spectrum

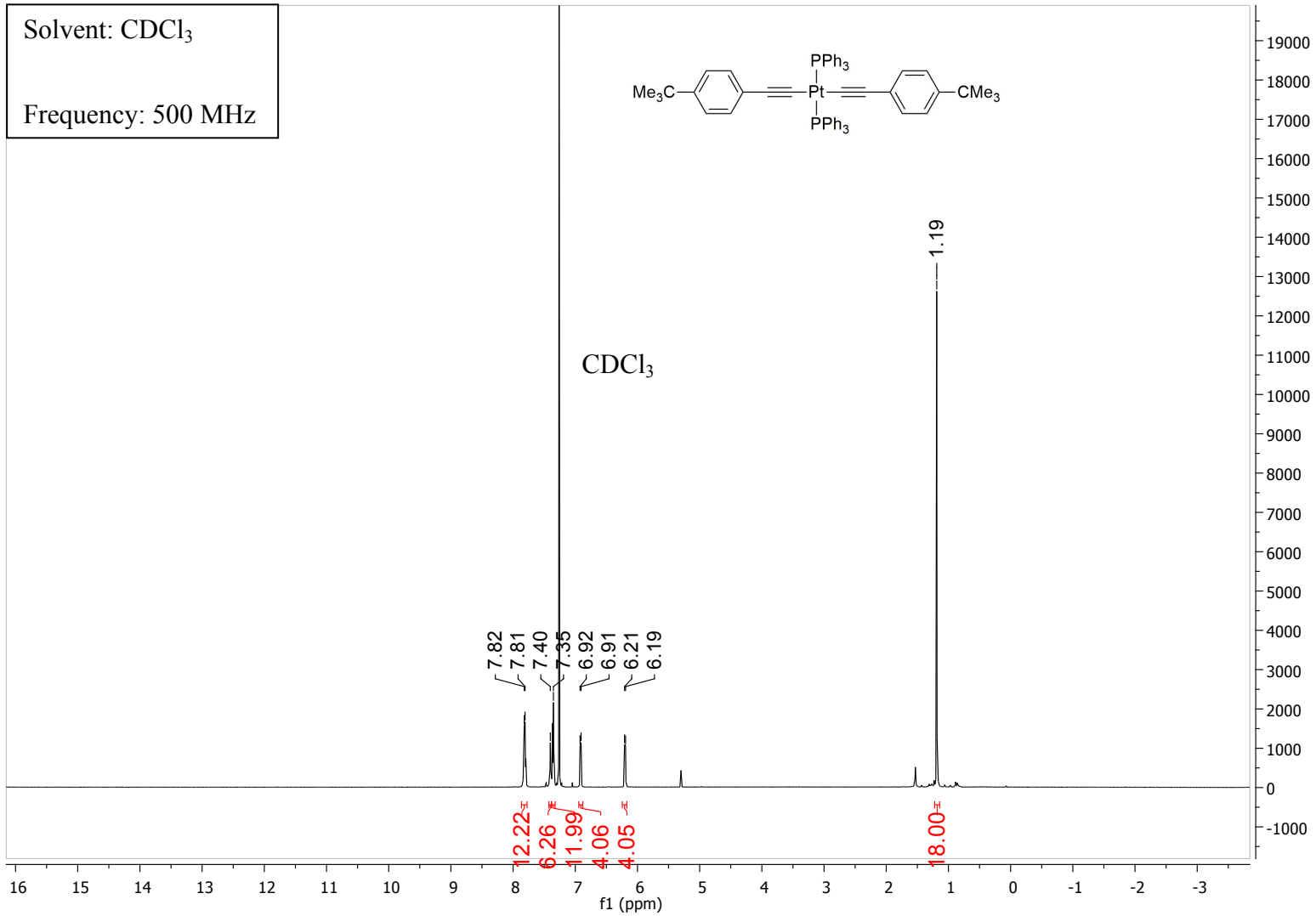

$^{31}P\{^{1}H\}$ NMR spectrum

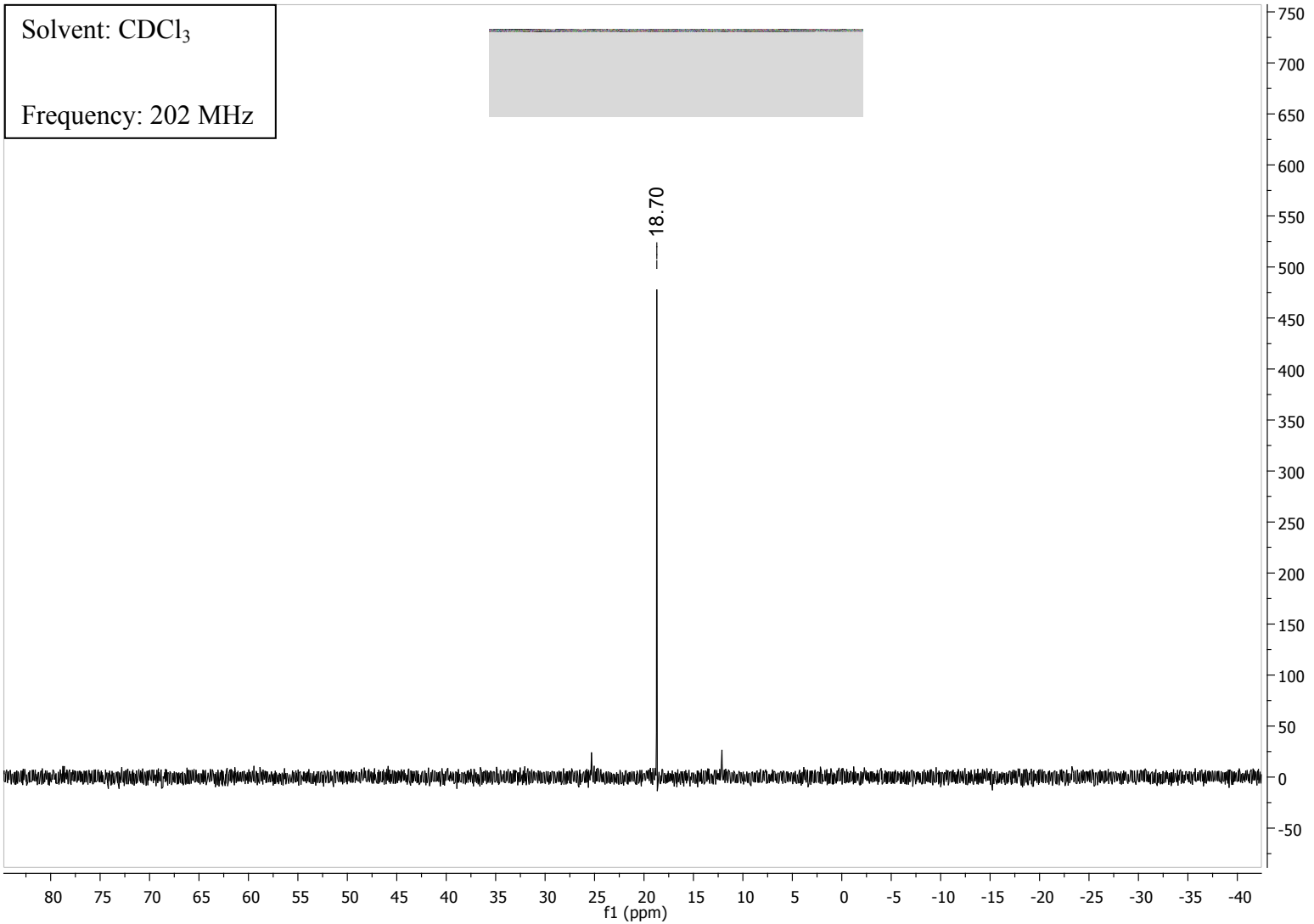

$^{13}C\{^{1}H\}$ NMR spectrum

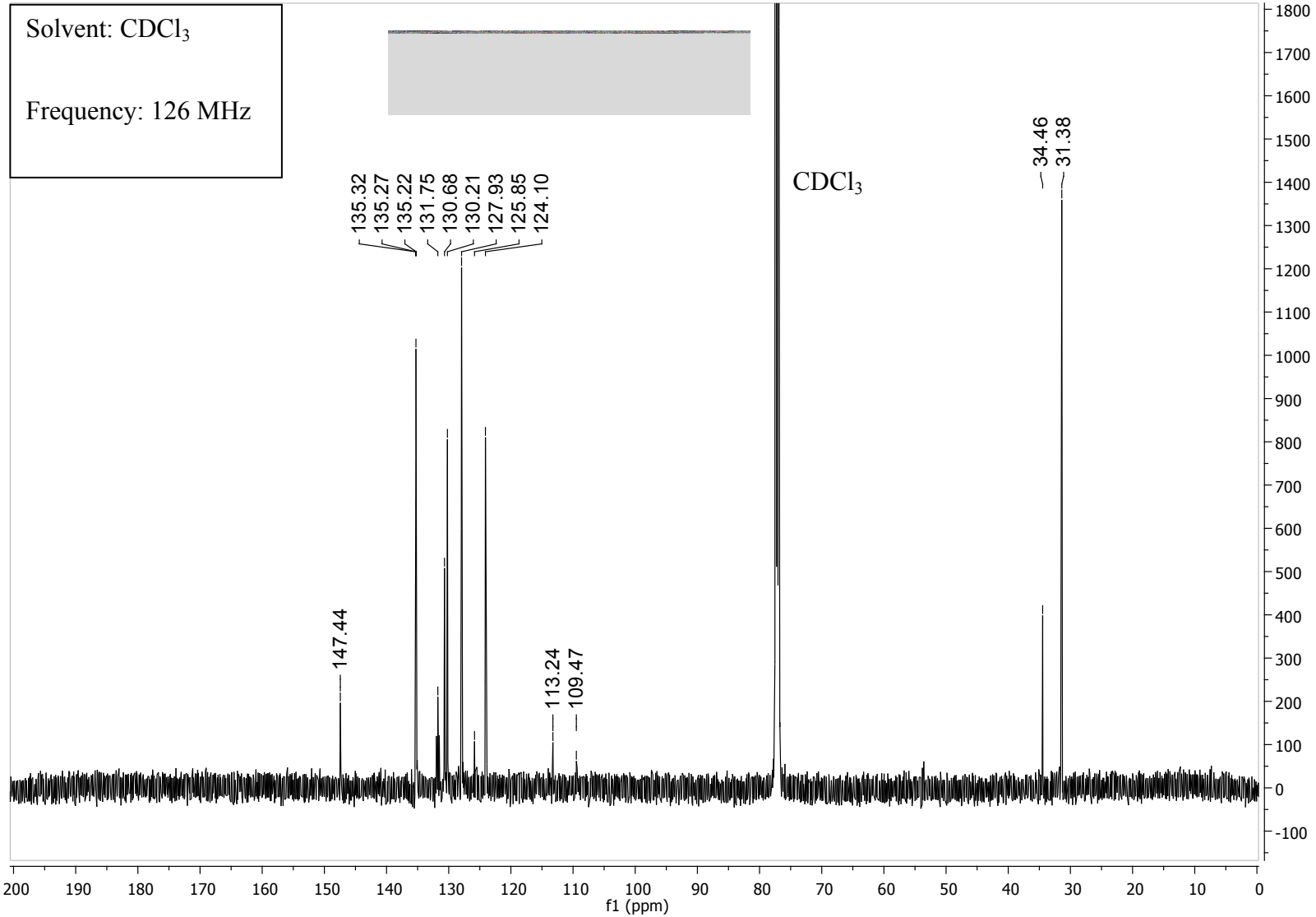

trans-Pt{C≡C-C_6H_4-CMe_3}$_2$(PEt_3)$_2$ (**4b**)

^{1}H NMR spectrum

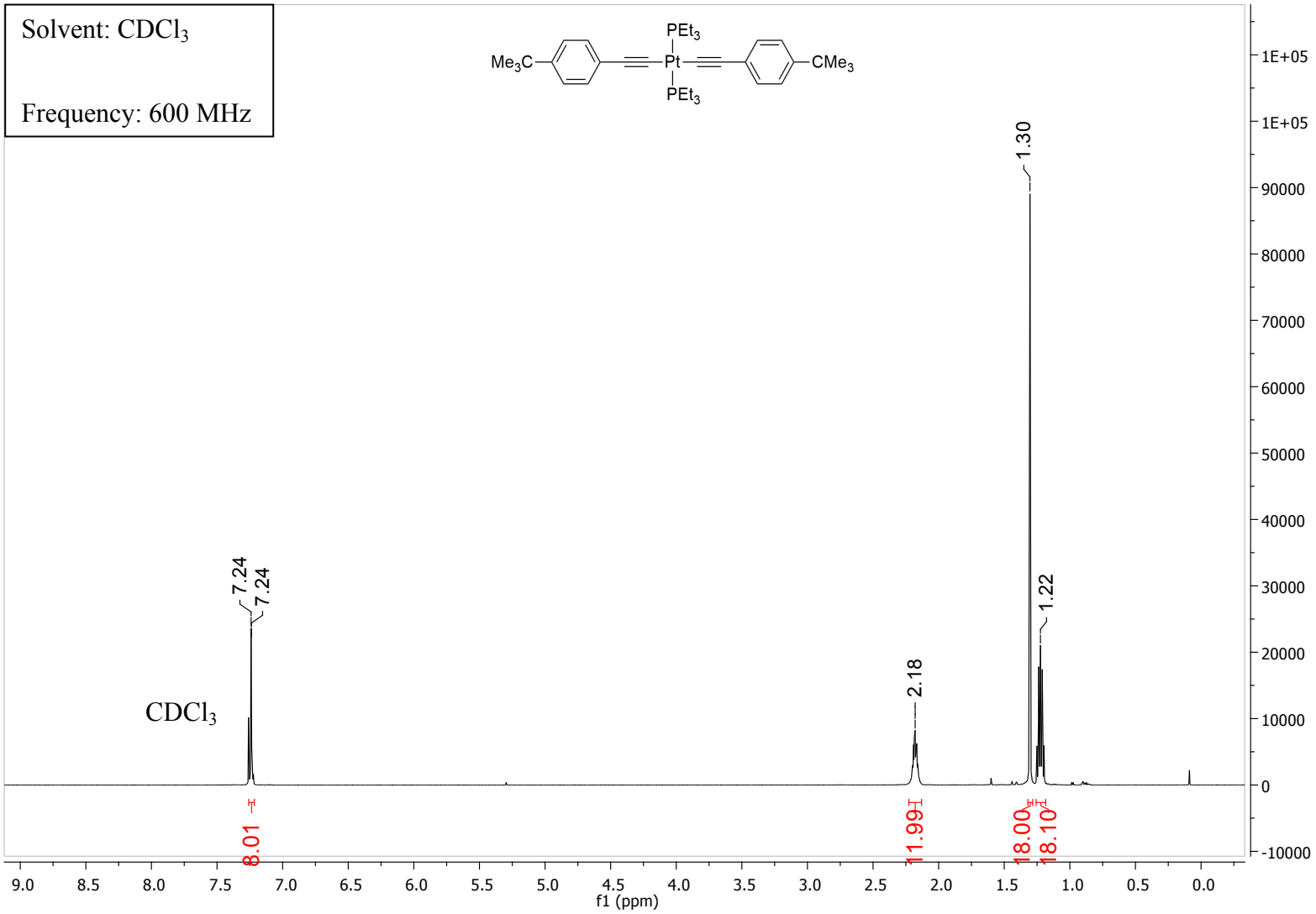

$^{31}P\{^{1}H\}$ NMR spectrum

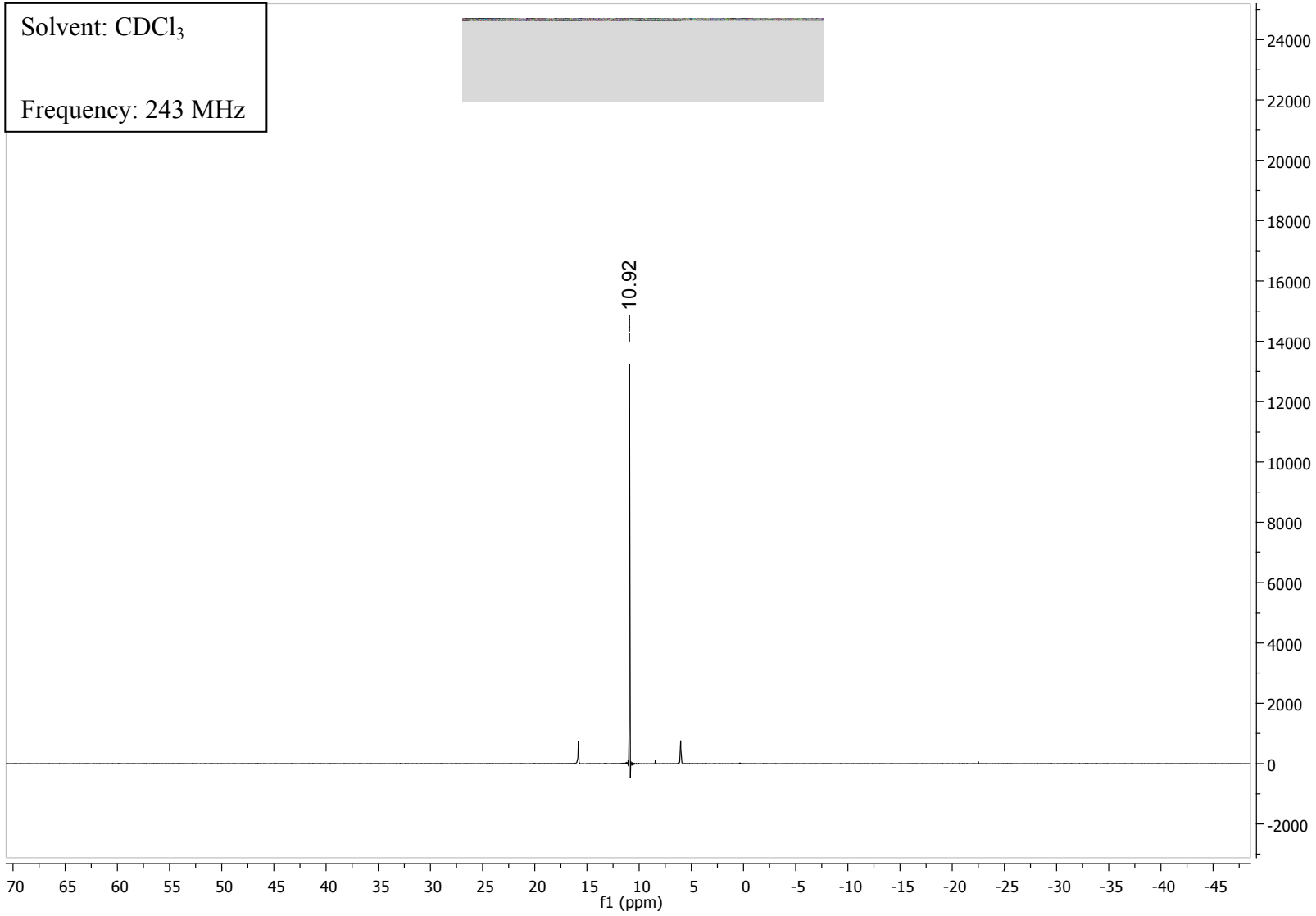

$^{13}C\{^{1}H\}$ NMR spectrum

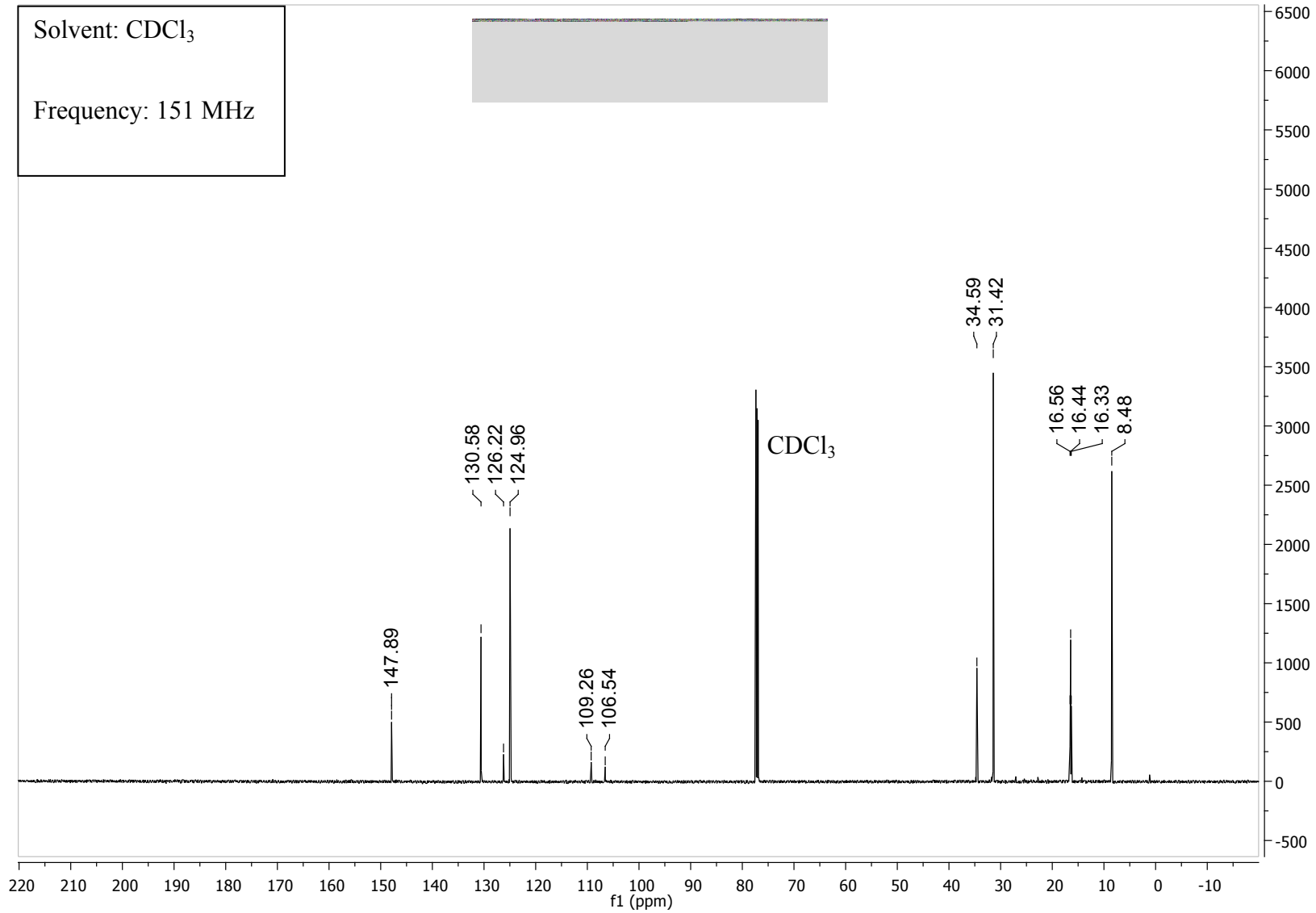

References

1 J. C. Bailar and H. Itatani, *Inorg. Chem.*, 1965, **4**, 1618–1620.
2 C. Z. Zhou, T. Liu, J. M. Xu and Z. K. Chen, *Macromolecules*, 2003, **36**, 1457–1464.
3 S. Marqués-González, M. Parthey, D. S. Yufit, J. A. K. Howard, M. Kaupp and P. J. Low, *Organometallics*, 2014, **33**, 4947–4963.
4 M. I. Bruce, P. J. Low, A. Werth, B. W. Skelton and A. H. White, *J. Chem. Soc. Dalton Trans.*, 1996, 1551–1566.
5 G. R. Fulmer, A. J. M. Miller, N. H. Sherden, H. E. Gottlieb, A. Nudelman, B. M. Stoltz, J. E. Bercaw and K. I. Goldberg, *Organometallics*, 2010, **29**, 2176–2179.
6 G. W. Parshall, *Inorg. Synth.*, 1970, **12**, 26–33.
7 D. E. Berry, *J. Chem. Educ.*, 1994, **71**, 899–902.
8 L. Bemi, H. C. Clark, J. A. Davies, C. A. Fyfe and R. E. Wasylishen, *J. Am. Chem. Soc.*, 1982, **104**, 438–445.
9 W. P. Power and R. E. Wasylishen, *Inorg. Chem.*, 1992, **31**, 2176–2183.
10 T. B. Peters, Q. Zheng, J. Stahl, J. C. Bohling, A. M. Arif, F. Hampel and J. A. Gladysz, *J. Organomet. Chem.*, 2002, **641**, 53–61.
11 G. M. Sheldrick, *Acta Crystallogr. Sect. C*, 2015, **71**, 3–8.
12 W. Haiss, D. Lackey, J. K. Sass and K. H. Besocke, *J. Chem. Phys.*, 1991, **95**, 2193–2196.
13 W. Haiss, H. Van Zalinge, S. J. Higgins, D. Bethell, H. Höbenreich, D. J. Schiffrin and R. J. Nichols, *J. Am. Chem. Soc.*, 2003, **125**, 15294–15295.
14 R. R. Ferradás, S. Marqués-González, H. M. Osorio, J. Ferrer, P. Cea, D. C. Milan, A. Vezzoli, S. J. Higgins, R. J. Nichols, P. J. Low, V. M. García-Suárez and S. Martín, *RSC Adv.*, 2016, **6**, 75111–75121.
15 S. Martín, W. Haiss, S. Higgins, P. Cea, M. C. López and R. J. Nichols, *J. Phys. Chem. C*, 2008, **112**, 3941–3948.
16 M. J. Frisch, G. W. Trucks, H. B. Schlegel, G. E. Scuseria, M. A. Robb, J. R. Cheeseman, G. Scalmani, V. Barone, G. A. Petersson, H. Nakatsuji, X. Li, M. Caricato, A. Marenich, J. Bloino, B. G. Janesko, R. Gomperts, B. Mennucci, H. P. Hratchian, J. V. Ortiz, A. F. Izmaylov, J. L. Sonnenberg, D. Williams-Young, F. Ding, F. Lipparini, F. Egidi, J. Goings, B. Peng, A. Petrone, T. Henderson, D. Ranasinghe, V. G. Zakrzewski, J. Gao, N. Rega, G. Zheng, W. Liang, M. Hada, M. Ehara, K. Toyota, R. Fukuda, J. Hasegawa, M. Ishida, T. Nakajima, Y. Honda, O. Kitao, H. Nakai, T. Vreven, K. Throssell, J. A. Montgomery, J. E. Peralta, F. Ogliaro, M. Bearpark, J. J. Heyd, E. Brothers, K. N. Kudin, V. N. Staroverov, T. Keith, R. Kobayashi, J. Normand, K. Raghavachari, A. Rendell and J. C. Burant, *Gaussian 09, Revision A, Gaussian*, Inc., 2009.
17 P. J. Stephens, F. J. Devlin, C. F. Chabalowski and M. J. Frisch, *J. Phys. Chem.*, 1994, **98**, 11623–11627.
18 A. D. Becke, *J. Chem. Phys.*, 1993, **98**, 5648–5652.
19 P. J. Hay and W. R. Wadt, *J. Chem. Phys.*, 1985, **82**, 299–310.
20 W. R. Wadt and P. J. Hay, *J. Chem. Phys.*, 1985, **82**, 284–298.
21 P. J. Hay and W. R. Wadt, *J. Chem. Phys.*, 1985, **82**, 270–283.
22 G. A. Petersson and M. A. Al-Laham, *J. Chem. Phys.*, 1991, **94**, 6081–6090.
23 N. M. O'Boyle, A. L. Tenderholt and K. M. Langner, *J. Comp. Chem.*, 2008, **29**,

839–845.
24 T. Markussen, M. Settnes and K. S. Thygesen, *J. Chem. Phys.*, 2011, **135**, 144104.
25 J. M. Soler, E. Artacho, J. D. Gale, A. García, J. Junquera, P. Ordejón and D. Sánchez-Portal, *J. Phys.: Condens. Matter*, 2002, **14**, 2745–2779.
26 J. Ferrer, C. J. Lambert, V. M. García-Suárez, D. Z. Manrique, D. Visontai, L. Oroszlany, R. Rodríguez-Ferradás, I. Grace, S. W. D. Bailey, K. Gillemot, H. Sadeghi and L. A. Algharagholy, *New J. Phys*, 2014, **16**, 093029.
27 C. J. Lambert, *Chem. Soc. Rev.*, 2015, **44**, 875–888.
28 D. Z. Manrique, C. Huang, M. Baghernejad, X. Zhao, O. A. Al-Owaedi, H. Sadeghi, V. Kaliginedi, W. Hong, M. Gulcur, T. Wandlowski, M. R. Bryce and C. J. Lambert, *Nature Commun.*, 2015, **6**, 6389.
29 R. Davidson, O. A. Al-Owaedi, D. C. Milan, Q. Zeng, J. Tory, F. Hartl, S. J. Higgins, R. J. Nichols, C. J. Lambert and P. J. Low, *Inorg. Chem.*, 2016, **55**, 2691–2700.
30 S. F. Boys and F. Bernardi, *Mol. Phys.*, 1970, **19**, 553–566.
31 C. Wang, A. S. Batsanov, M. R. Bryce, S. Martín, R. J. Nichols, S. J. Higgins, V. M. García-Suárez and C. J. Lambert, *J. Am. Chem. Soc.*, 2009, **131**, 15647–15654.